JCI The Journal of Clinical Investigation

Tetracyclines improve experimental lymphatic filariasis pathology by disrupting interleukin-4 receptor-mediated lymphangiogenesis

Julio Furlong-Silva, … , Mark J. Taylor, Joseph D. Turner

J Clin Invest. 2021. https://doi.org/10.1172/JCI140853.

Research In-Press Preview Infectious disease Inflammation

Graphical abstract

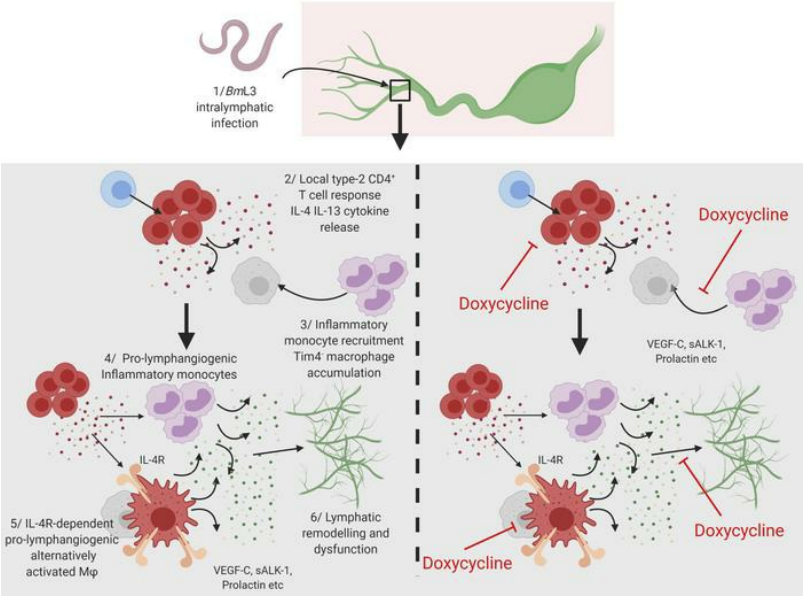

Find the latest version:

https://jci.me/140853/pdf

Tetracyclines improve experimental lymphatic filariasis pathology by disrupting interleukin-4 receptor-mediated lymphangiogenesis

Authors: Julio Furlong-Silva[1], Stephen D Cross[1], Amy E Marriott[1], Nicolas Pionnier[1], John Archer[1], Andrew Steven[1], Stefan Schulte Merker[2], Matthias Mack[3], Young-Kwon Hong[4], Mark J Taylor[1] and Joseph D Turner[1*]

Affiliations:

[1]Centre for Drugs & Diagnostics, Department of Tropical Disease Biology, Liverpool School of Tropical Medicine, Pembroke Place, Liverpool L3 5QA, UK

[2]Institute for Cardiovascular Organogenesis and Regeneration, Faculty of Medicine, WWU Münster, Mendelstraße 7, 48149 Münster, Germany

[3]Universitätsklinikum Regensburg, 93053 Regensburg, Germany

[4]Department of Surgery, Norris Comprehensive Cancer Center, Keck School of Medicine, University of Southern California 1450 Biggy St. NRT6501, M/C9601, Los Angeles, CA 90033

* Corresponding author contact details:

email: joseph.turner@lstmed.ac.uk

Telephone: +44 (0)151 7053119

This work was funded by public and charitable agencies that require a Creative Commons CC-BY license in order for publication costs to be met.

Funding: This work was supported by a Medical Research Council New Investigator Research Grant (MR/L018756/1) to JDT, a Bill and Melinda Gates Grant (OPP1054324) and a Wellcome Foundation Trust Equipment Grant (104936/Z/14/Z) to JDT and MJT. The funding bodies had no roles in the design of the study and collection, analysis, and interpretation of data.

The authors have declared that no conflict of interest exists

One Sentence Summary:

Tetracyclines improve experimental filariasis lymphatic pathology by targeting multiple aspects of an interleukin-4 receptor type-2 inflammatory pathway of lymphangiogenesis in a preclinical filarial disease model.

Abstract

Lymphatic filariasis is the major global cause of non-hereditary lymphedema. We demonstrate the filarial nematode, *Brugia malayi,* induces lymphatic remodelling and impaired lymphatic drainage following parasitism of limb lymphatics in a mouse model. Lymphatic insufficiency was associated with elevated circulating lymphangiogenic mediators, including vascular endothelial growth factor C. Lymphatic insufficiency was dependent on type-2 adaptive immunity, interleukin-4 receptor, recruitment of C-C chemokine receptor-2 monocytes and alternatively-activated macrophages with pro-lymphangiogenic phenotype. Oral treatments with second-generation tetracyclines improved lymphatic function, while other classes of antibiotic had no significant effect. Second-generation tetracyclines directly targeted lymphatic endothelial cell proliferation and modified type-2 pro-lymphangiogenic macrophage development. Doxycycline treatment impeded monocyte recruitment, inhibited polarisation of alternatively-activated macrophages and suppressed T cell adaptive immune responses following infection. Our results determine a mechanism-of-action for the anti-morbidity effects of doxycycline in filariasis and supports clinical evaluation of second-generation tetracyclines as affordable, safe therapeutics for lymphedemas of chronic inflammatory origin.

55

56

57 **Graphical abstract**

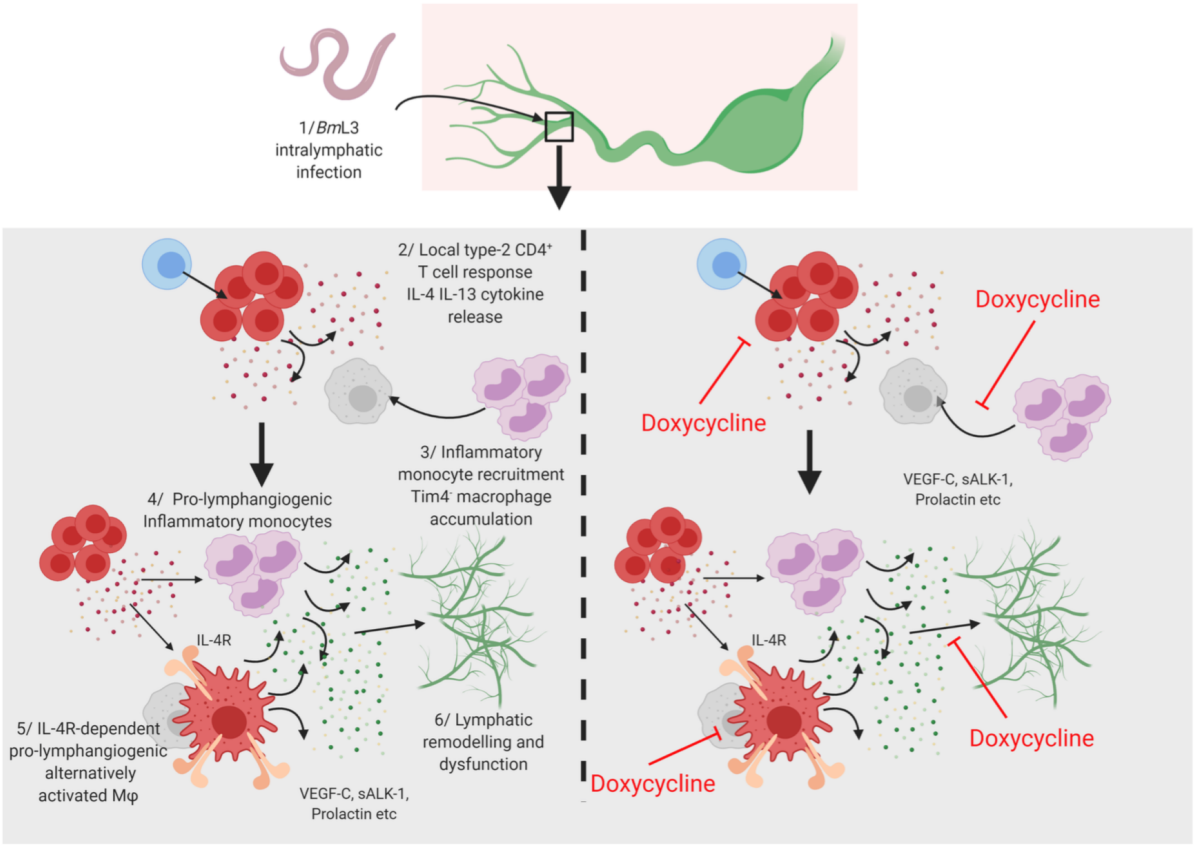

58

59

Introduction

Lymphedema (LE) affects 200 million individuals worldwide (1). LE is caused by disruption of normal lymphatic function whereby return drainage of fluid, proteins, fats and immune cells (lymph) is impaired (2). LE is either hereditary, caused by mutations in genes controlling lymphatic development, or non-hereditary, caused by infection, trauma or surgical removal of lymphatics to prevent cancer metastasis (2, 3). The major cause of secondary LE is lymphatic filariasis (LF), a neglected tropical disease infecting an estimated 67 million people with a further 890 million at risk (4). Filarial LE causes life-long physical and associative mental disability (5), ranking LF as the 4th highest contributor to global disability adjusted life years. Tangible progress has been made in LF elimination via mass drug administration of anti-filarial drugs, effectively halving the number of active infections between 2000 and 2013 (4), whereas numbers of LE patients has remained static at 40 million over the same time-period. Current treatment for filarial LE is limited to 'morbidity management and disability prevention', which involves a package of hygiene measures and implementation of physiotherapy in the household (6). No chemotherapeutic interventions are indicated for filarial LE. However, antibiotics are recommended to treat secondary skin bacterial infections which can reduce the frequency of periodic inflammatory episodes, known as acute dermatolymphangioadenitis (ADLA), a form of cellulitis. In a recent placebo-controlled clinical trial, whilst both amoxicillin (the standard antibiotic treatment for ADLA) and doxycycline reduced the frequency of ADLA, doxycycline also showed surprising efficacy in reversing LE grade (7).

Lymphatic remodelling is a hallmark of filarial LE, with clearly established evidence from *in vitro* (8, 9)*, in vivo* (10–13) and clinical (14–16) studies. How lymphatic remodelling develops and its role in LF pathology is poorly understood.

In this study, we develop a novel murine hind-limb model of filarial infection, utilising longitudinal intravital imaging to demonstrate filarial infective larvae induce rapid lymphatic alterations, associated with induction of lymphatic insufficiency. We demonstrate that early filarial lymphatic pathology is primarily host-immune driven, characterising an interleukin-4 receptor (IL-4R) 'type-2' dependent axis involving recruitment of inflammatory monocytes and

alternatively-activated macrophages (AAMϕ) that promote the development of lymphatic disease. We demonstrate that second generation tetracyclines can target multiple aspects of this pathway to ameliorate lymphatic pathology.

Results

Brugia malayi infection induces lymphatic remodelling and dysfunction

We developed a murine lymphatic pathology model whereby C57BL/6J mice were administered with subcutaneous inoculations of *B. malayi* infective third stage larvae (*Bm*L3) to the left hind-limb (Figure 1A). We confirmed filarial larvae established intra-lymphatic infections by imaging motile, fluorescently labelled *Bm*L3 within GFP-tagged Prox-1^{+} collecting vessels (lymphangions) of the infected hind-limb (Figure 1B and Supplemental Movie 1). Motile *Bm*L3 could be observed within superficial dermal lymphatics from 3 hours to 4 days post-infection. Near-infrared intravital indocyanine green (ICG) lymphography was undertaken to investigate the impact of *B. malayi* larval infection on lymphatic structure and function (Figure 1A, Supplemental Figure 1 and Supplemental File 1). Clinical ICG lymphography has characterised “splash”, “stardust” and “diffuse” dermal backflow patterns, and visualisation of tortuous collateral lymphatics, associated with onset of LE in patients (17). At two-weeks post-*B. malayi* infection, we observed the presence of all three dermal backflow patterns and tortuous collateral lymphatic development (Figure 1C, Supplemental Figure 2A-B). By image analysis we determined *Bm*L3-infected C57BL/6J mice displayed significant levels of lymphatic remodelling in dorsal, lateral and ventral aspects of the infected limb (Figure 1C-D). Remodelling was pronounced at sites proximal to initial invasion of the superficial lymphatics, although by this time-point there was no evidence of motile intra-lymphatic larvae. By epi-fluorescent imaging, we could detect significant, mean two-fold dilations of Prox-1^{+} lymphatic vessels at two weeks-post infection (Figure 1E-F). By comparing ICG dermal backflow in infected and uninfected limbs, significant ICG retention was evident in the infected limbs, compared to sham-controls (Figure 1G). Further, in an Evan’s Blue (EB) dermal retention assay (Supplemental Figure 1) significant EB accumulation in the skin of *Bm*L3 infected limbs was discerned (Figure 1H). Repeat experiments using BALB/c mice demonstrated that all aspects of lymphatic pathology were reproducible on this background strain, although to a generally lower degree of severity (Supplemental Figure 2).

Because inbred mice mount an effective adaptive immune response to control *B. malayi* infection before chronic adult intra-lymphatic filarial parasitism can establish (18), we next investigated if infection-induced lymphatic remodelling and dysfunction resolved post-clearance of filarial infection. *Bm*L3 infected mice imaged at 16 weeks post-infection retained backflow and tortuous lymphatic patterning, with no significant decline in lymphatic remodelling or levels of lymphatic insufficiency, compared to 2 weeks post-infection (Figure 1C,I-J). At 16 weeks-post infection, there was no evidence of active intra-lymphatic adult parasitism or circulating microfilariae, indicating lymphatic pathology persists long-term after initial induction by filarial infection.

To explore host molecular mechanisms mediating filarial lymphatic pathology, we compared circulating plasma concentrations of a focused array of angiogenic / lymphangiogenic factors between 14dpi *Bm*L3 and sham infected cohorts. A milieu of lymphangiogenic factors were upregulated in *Bm*L3 infected mice including: Vascular endothelial growth factor-C (VEGFC), soluble activin receptor like kinase-1 (sALK-1) and prolactin (Figure 2A-B). As VEGFC is a well characterised primary lymphangiogenic mediator (19), we investigated the impact of isolated VEGFC delivery to the hind-limb skin-draining lymph nodes (sdLN).

We administered a VEGFC expressing adenoviral vector (adVEGFC) to increase local VEGFC signalling in the same anatomical areas exposed to *Bm*L3 infection. AdVEGFC treated groups displayed significantly higher levels of both lymphatic remodelling and insufficiency, compared to both naïve and GFP expressing adenoviral vector (adGFP) treated control mice, with mid-dose adVEGFC administration recapitulating magnitudes of lymphatic remodelling and pathology comparable to 14d *Bm*L3 infected mice (Supplemental Figure 3).

Filarial lymphatic pathology is dependent on IL-4 receptor type-2 adaptive immune responses

Previous clinical studies have demonstrated a link between symptomatic LF and enhanced parasite-specific host adaptive immune responses (20, 21). In mice, a polarised ‘type-2’ adaptive immune response coordinates effective eosinophilic-mediated immunity against larval-stage filariae (22). We investigated the role of adaptive immunity by comparing magnitudes of lymphatic remodelling and insufficiency between WT and Severe Combined

Immunodeficient (SCID) mice lacking functional B and T lymphocytes. *Bm*L3-infected CB.17 (BALB/c congenic) SCID mice displayed muted levels of lymphatic remodelling which were not significantly different compared to sham controls and significantly lower than corresponding BALB/c WT infections assessed at either 2- or 5-weeks post-infection (Figure 3A-B). Concomitantly, no significant difference in lymphatic insufficiency was observed between sham and infected SCID mice, judged by either ICG or EB dermal backflow at 2-weeks post-infection (Figure 3C-D). We then characterised the localised $CD4^+$T cell adaptive immune response in sdLN and major afferent lymphatic collecting vessels proximal to filarial parasitized and remodelled lymphatic tissues, utilising intracellular cytokine flow cytometry (Supplemental Figure 4). Significant expansions of 'type-2' interleukin (IL)-4 and IL-13 secreting $CD4^+$ T-cells were observed in sdLN single cell suspensions derived from *Bm*L3 infected mice at 14 dpi and $CD4^+$ secretion levels of the regulatory-type cytokine, IL-10, was also increased, whilst local secretion levels of the 'type-1' cytokine, inferferon-γ, remained unaltered following infection (Figure 2E-F). Subsequently, we tested whether ablation of type-2 immune signalling would impact on the severity of filarial lymphatic pathology, utilising IL-4 receptor alpha (IL-4Rα) deficient mice, unable to respond to either IL-4 or IL-13. Following *Bm*L3 infection, IL-4Rα knockout mice (IL-4R$\alpha^{-/-}$), on either BALB/c or C57BL/6 backgrounds, exhibited significantly diminished lymphatic remodelling and lymphatic dysfunction (Figure 4A-D). Levels of circulating lymphangiogenic mediators were also significantly abrogated in IL-4R$\alpha^{-/-}$ *Bm*L3 infected mice, notably VEGF-C and angiopoetin-2 (Figure 4E-F). This data indicates a functional role for IL-4R-dependent type-2 adaptive immune responses in the induction of early filarial lymphatic pathology.

Pro-lymphangiogenic inflammatory monocytes and alternatively-activated macrophages are mediators of filarial lymphatic dysfunction

We investigated the contribution of local cellular inflammatory responses in mediating filarial lymphatic pathology. By immunophenotyping the sdLN and major afferent lymphatic collecting vessels proximal to *Bm*L3 inoculation sites, we determined significant expansions of

CD11b^{+}Ly6C^{+}CCR2^{+} 'inflammatory' monocyte and CD11b^{+}F480^{+}MHCII^{+} MΦ populations (Figure 5A-B), significant eosinophilic and neutrophilic granulocyte recruitments and T and B lymphocyte proliferations (Supplemental Figure 5). In the absence of functional IL-4Rα signalling, a slight decrease in monocyte recruitment was observed and lymphatic-tissue MΦ expansions were significantly impeded following filarial infection (Figure 5A-B). A significant, 2-fold reduction in MΦ expressing the tissue residency marker, Tim-4 (23), in filarial infected WT but not IL-4Rα$^{-/-}$ mice was apparent (Figure 5C-D), suggestive of IL-4R-dependent recruitment of monocyte-derived MΦ within the expanded lymphatic-tissue MΦ pool, post *Bm*L3 infection. Filarial-infection expanded lymphatic-tissue MΦ also displayed significantly increased expression of the AAMΦ markers, RELM-α and CD206 (mannose receptor; a specific marker of alternative activation within monocyte-differentiated MΦ in cardiac and hepatic tissues) (24, 25) (Figure 3C-D). AAMΦ development post-filarial infection in proximal lymphatic tissues was completely abrogated in the absence of intact IL-4R signalling (Figure 3C-D). AAMΦ polarisation is a well characterised hallmark of filarial infection (26), and IL-4-stimulated AAMs are important in mediating filarial expulsion by sustaining recruitment of eosinophils (22). Because Mϕ are potent cellular mediators of angiogenesis and lymphangiogenesis (27), we explored the lymphangiogenic phenotype of purified monocytes and macrophages from lymphatic tissues post-filarial infection. Cell-sorted CD11b^{+}Ly6C^{+}CCR2^{+} inflammatory monocytes secreted significantly higher concentrations of: prolactin, sALK-1, IL-6 and amphiregulin, while CD11b^{+}F480^{+}MHCII^{+} MΦ secreted significantly higher levels of VEGF-C compared to sham-infected controls (Figure 3E). In a tandem approach, we examined the direct pro-lymphangiogenic potential of type-2 cytokine or filarial-stimulated human THP-1 monocyte-derived MΦ. For this we developed a human dermal lymphatic endothelial cell (LEC) proliferation assay following co-culture with monocyte-derived MΦ macrophages pre-conditioned with recombinant (r)IFN-γ, rIL-4+rIL-13, live *Bm*L3 or *Bm*L3 extract (*Bm*L3E) (Figure 6A). rIL-4+rIL-13, live *Bm*L3 and *Bm*L3E conditioned macrophages mediated significant LEC proliferation compared with either LEC cells cultured

in basal media alone, or in the presence of naïve THP1 monocyte derived MΦ (Figure 6B). Analysis of conditioned media from rIL-4+rIL-13 stimulated monocyte-derived MΦ revealed significantly elevated levels of pro-lymphangiogenic mediators: VEGFA, Follistatin, and Human Growth Factor (HGF) (Figure 6C), while significantly elevated VEGFC and HGF were observed in *Bm*L3E-pulsed MΦ conditioned media (Figure 6D). This human co-culture system confirmed monocyte-derived MΦ exposed to both a type-2 dominated (IL-4+IL-13) microenvironment and filarial-specific antigenic stimuli polarise toward a lymphangiogenic phenotype, capable of inducing the proliferation of LECs.

To interrogate the functional role of pro-lymphangiogenic monocytes and monocyte-derived MΦ recruited to the site of filarial-parasitised lymphatics, we blocked CCR2 monocyte recruitment following *Bm*L3 infection by administration of an anti-CCR2 (α-CCR2) ablating antibody (28). In a complementary approach, we reduced total phagocyte cell populations, including monocytes and Mϕ, by local subcutaneous administration of clodronate-encapsulated liposomes (CL) (Figure 7A). Confirming treatment efficacy, both α-CCR2 and CL treatments delivered to filarial infected mice successfully reduced circulating blood monocyte populations. Further, α-CCR2 significantly reduced lymphatic-associated monocyte populations following infection (Figure 7B-C). Following ablations of monocyte and total phagocyte populations, whilst remodelled lymphatics were still apparent, the magnitude of lymphatic insufficiency was significantly reduced, demonstrated by reduced backflow of ICG following α-CCR2 treatment (Figure 7F-G) and dermal retention of EB (Figure 7H) following both α-CCR2 and CL treatments. Additionally, dermal lymphatic vessel dilation was significantly reduced following both α-CCR2 and CL treatments (Figure 7I-J). These ablation experiments indicate a functional role for pro-lymphangiogenic monocyte populations, post-recruitment from the blood to local parasitized lymphatics, in the development of filarial-associated lymphatic dysfunction.

Second generation tetracyclines target IL-4 receptor-dependent macrophage lymphangiogenesis to ameliorate filarial lymphatic pathology.

With previous work demonstrating anti-morbidity efficacy of the second generation tetracycline; doxycycline, in the treatment of filarial LE (7, 16, 29), we established whether our preclinical filarial-lymphatic pathology model was responsive to oral doxycycline intervention. After 14-days infection and co-treatment with a doxycycline regimen bioequivalent to human 200mg daily oral dosing (30) (Figure 8A), mice exhibited significantly lower levels of both lymphatic remodelling (Figure 8B-C) and lymphatic insufficiency compared with infected and vehicle control animals (Figure 8D-E). We did not observe direct anti-filarial efficacy at these treatment dose ranges against *B. malayi* developing larvae up to 14 days, ruling out a direct anti-parasitic mode-of-action contributing toward reduced pathology (Supplemental Figure 6). Because the filarial endosymbiont, *Wolbachia,* is depleted by tetracyclines (30, 31) and can trigger innate inflammation via ligation of surface lipoproteins by toll-like receptor two and six heterodimers (TLR2/6) (32), we investigated whether initiation of lymphatic pathology was influenced by *Wolbachia.* In addition, using the related second-generation antibiotic, minocycline, and a selection of different classes of antibiotic, we tested whether suppression of lymphatic pathology was a phenomenon unique to the tetracycline class or could be mediated by other antibiotics with anti-*Wolbachia* and/or broad-spectrum antibacterial activities (Figure 9A). We selected high dose rifampicin as a broad-spectrum antibiotic with superior anti-*Wolbachia* activity compared to tetracyclines (33), as well as amoxicillin and chloramphenicol; both potent, broad-spectrum antibiotics lacking significant anti-*Wolbachia* activity (34). Similar to effects observed with doxycycline, minocycline, delivered at doses bio-equivalent to 100mg human oral exposures (30), led to significantly improved severity of lymphatic remodelling and insufficiency (Figure 9B-D). Comparatively, none of the other administered broad-spectrum antibiotics: amoxicillin, chloramphenicol or rifampicin, had any significant effect on either lymphatic remodelling or insufficiency following filarial lymphatic infection (Figure 9B-D). Filarial-infected TLR-6 deficient mice displayed no significant difference in either magnitude of lymphatic remodelling or lymphatic insufficiency compared to WT controls (Figure 9E-G). Together, this data defines a specific anti-morbidity efficacy of

second generation tetracyclines in ameliorating filarial-induced lymphatic pathology, independent of general antibiotic or anti-*Wolbachia* specific modes-of-action.

We tested which facets of the type-2 inflammatory lymphangiogenic pathway induced by filarial infection were targeted by tetracyclines. We first investigated whether doxycycline could directly affect lymphangiogenesis *in vitro*. Growth assays, utilising time-lapse microscopy to longitudinally quantify LEC or tissue-equivalent adult human dermal microvascular vascular endothelial cell (blood endothelial cell; BEC) proliferation over nine days were performed (Supplemental File 2). Treatment of LEC or BEC with 10-20μM doxycycline impeded proliferation in response to a VEGFA stimulus, in a dose dependent manner (Figure 10A-B; Supplemental File 2). Similar effects were obtained with BECs and LECs treated with minocycline (Supplemental Figure 7). We then treated monocyte-derived Mϕ with 10μM doxycycline simultaneously during stimulation with live *Bm*L3, *Bm*L3 with type-2 cytokines or *Bm*L3 extract. Mϕ were washed before their transfer within trans-wells onto LEC cultures to remove drug (Figure 10C). Whilst rIL4+rIL13-, *Bm*L3+rIL4+rIL13- and *Bm*L3E-pulsed Mϕ mediated significant LEC proliferation, this affect was abolished by pre-treatment with doxycycline (Figure 10D). Addition of 10μM doxycycline to *Bm*L3E-pulsed Mϕ and LEC co-cultures also abrogated LEC proliferation (Figure 10E). No significant cytotoxicity was discerned when LEC or THP-1 Mϕ were exposed to 10-20μM doses of doxycycline and LEC cultures responded to VEGF proliferating stimulus following removal of drug (Supplemental Figure 8). These *in vitro* data indicate that second-generation tetracyclines reversibly suppress VEGF-mediated lymphangiogenesis and, independently, the development of pro-lymphangiogenic monocyte-derived Mϕ following filarial and/or type-2 cytokine stimulations. Using the filarial lymphatic pathology mouse model, we immuno-phenotyped lymphatic-associated myeloid cells from mice orally dosed with doxycycline compared with infection vehicle-dosed controls. Doxycycline treated mice displayed significantly impeded monocyte recruitment compared to infection controls whilst lymphatic-associated MΦ populations failed to expand (Figure 11A). Eosinophil levels in lymphatic tissues were also significantly reduced

in infected mice following doxycycline treatment (Figure 11A). Doxycycline treatment also significantly blocked AAMϕ polarisation as measured by reduced populations of RELMα^{+} MΦ (Figure 11B-C). We examined if this modified myeloid cell recruitment and reduced AAMϕ lymphangiogenic potential resulted in reduced local concentrations of the lymphangiogenic milieu. *Ex vivo* culture of single cell suspensions prepared from sdLN and adjacent lymphatic channels of filarial-infected mice treated with doxycycline demonstrated reductions in multiple lymphangiogenic secretions compared to infection controls (Figure 11D). Follistatin was significantly reduced, whilst VEGF-C secretions remained at sham-infection control levels (Figure 11E). We then examined whether the initial, predominant type-2 adaptive immune response important for mediating lymphatic pathology was perturbed by doxycycline. We assessed splenocyte recall assays to evaluate systemic immune responses. Doxycycline treatments modified numerous cytokines, compared to *Bm*L3 infection alone (Figure 11F-G). Reductions in secretions of type-2 cytokines: IL-3, IL-4, IL-9 and IL-5 were observed post-doxycycline treatment in infected mice. Additionally, modified systemic type-1 (IFNγ) and type-17 (IL-17) splenocyte secretions were recorded post-doxycycline treatment. Further, general reductions in chemokine production, including those responsible for monocyte and macrophage activation (CXCL2, G-CSF), as well as the pro-lymphangiogenic growth factor, VEGF-A, were observed within splenocytes, post-doxycycline treatment (Supplemental Figure 9). Therefore, second-generation tetracyclines target multiple aspects of the type-2 inflammatory lymphangiogenic axis induced by filarial larval infection, as well as directly targeting lymphatic endothelial proliferation, to modify lymphatic filarial disease.

Discussion

We reveal persistent lymphatic dilation, remodelling and dermal backflow patterns in mice that emulate clinical lymphatic remodelling in both filarial and non-filarial LE patients (14–17). Further, we record significant upregulation of the pro-lymphangiogenic circulating factors, Ang2, TNFα and VEGFC, which are clinical serological markers of filariasis infection and LE pathology (29, 35, 36). Thus, we conclude that our preclinical model is representative of early lymphatic pathological changes in filariasis patients and a useful tool to interrogate the pathophysiology and therapeutic targeting of filarial disease.

Our model revealed that, surprisingly, abbreviated larval filarial infections, in as little as 6 days, could rapidly induce enduring lymphatic pathology without the necessity for establishment of chronic adult infections. It is currently not known whether such rapid pathology is evident in humans as markers of adult filarial infection are typically utilised as selection criteria for study. However, a recent investigation has defined via lymphoscintigraphy that lymphatic pathology is evident in children as young as five (37). Thus, we contend that frequent larval assaults transmitted by mosquito bites, that do not necessarily result in patent adult infections, may cause under-appreciated lymphatic pathology in LF endemic areas.

Strain-dependent magnitude of lymphatic remodelling, whereby BALB/c mice exhibited reduced pathology compared with C57BL/6 mice, reflects the relative vigour of sterilising immunity against filarial infection between these two strains (38). Indeed, severity of LE in filariasis patients is associated with magnitude of CD4+ T cell immune responses to filarial antigen (20). In our model, local draining lymph node adaptive immune responses were polarised toward IL-4 and IL-13 CD4+ secretion, suggesting an important role for type-2 sterilising immune responses in induction of lymphatic dysfunction. We have defined eosinophil coordinated type-2 immune responses are critical to prevent *B. malayi* larval survival (22, 39). Lymphatic remodelling and dysfunction were reduced in SCID mice following filarial infection, demonstrating a requirement for adaptive immunity to induce early lymphatic dysfunction.

A Limitation of our study was that whilst lymphatic pathology was rapidly induced, we did not observe overt LE in immuno-competent mice following a single infection event and up to 16 weeks follow-up. Further, we used a single high dose infection (100 L3) whereas humans will be naturally exposed repetitively to low doses of typically <10 L3 in 'trickle infections'. Whilst dilation of *B. malayi* adult parasitized lymphatics and LE formation has been documented in *B. malayi* susceptible T cell immune-deficient mice (11, 13), reactivation of adaptive immunity during chronic infection time-courses in aged mice was not scrutinised in these 'leaky' lymphopenic models. Indeed, experimental immune reconstitution triggers a destructive, fibrotic, peri-lymphangitis pathology with myeloid-rich infiltrates in infected lymphatics co-incident with immune-killing of adult parasites (11). Further, in experimental infections of outbred feline and canine natural *Brugia* hosts, overt LE is associated with leukocytic intra-lymphatic obstructive thrombi and exacerbated by bacterial or fungal secondary infections (40, 41). In a susceptible ferret model of *B. malayi* infection, six trickle-dose inoculations over a ten-week period resulted in overt LE in one out of four animals tested (12). Thus, we suggest the immediate adaptive immune-dependent lymphatic pathology we detail is an early facet of a complex multi-factorial process, likely requiring several chronic infection events within the limb lymphatic network and prime-boosting of type-2 immunity to culminate in pronounced lymphedematous disease.

In non-filarial LE models, CD4+ T cell depletion reduces lymphatic pathology, whilst specific neutralisation of type-2 cytokines, IL-4 and IL-13, ameliorates oedematous skin fibrosis (42, 43). Confirming the importance of type-2 immunity in filarial lymphatic pathology, IL-4 receptor deficient mice did not develop significant remodelling and were protected from lymphatic dysfunction post-infection. IL-4R deficiency resulted in: reductions in multiple circulating lymphangiogenic factors, notably VEGFC and Ang2, reduced monocyte / Mϕ expansions within parasitized lymphatics and prevention of Mϕ alternative activation. We, and others, have previously described IL-4 receptor-dependent alternative activation of serous-cavity tissue Mϕ populations in the context of filarial infection (22, 44). In oncology, dysregulated, tumour-

358 derived stimuli polarises monocytes and macrophages into “tumour-associated” phenotypes,
359 possessing similarities to AAMϕ, and resulting in increased tumour angiogenesis and
360 lymphangiogenesis (45). In clinical filariasis, circulating monocytes with features of alternative
361 activation have also been detected (46). We determined that lymphatic-associated monocytes
362 and AAMϕ from parasitized tissues produced elevated VEGFC, sALK-1 and prolactin, the
363 three most upregulated pro-lymphangiogenic molecules in circulation following filarial
364 infection, demonstrating this cell lineage are cellular sources of lymphangiogenic mediators at
365 the site of filarial lymphatic pathology. Clinically, it has been shown that circulating blood
366 mononuclear cells derived from filarial LE patients also demonstrate heightened VEGFA/C
367 production upon *ex vivo* stimulations with either TLR or filarial antigens (47).
368 By serial depletion of CCR2+ monocytes or total phagocytes *in vivo*, we confirmed temporal
369 monocyte deficiency and impaired lymphatic recruitment alleviated lymphatic dysfunction and
370 reduced lymphatic dilation. Similarly, CCR2 monocyte recruitment has been demonstrated to
371 mediate intestinal inflammatory lymphangiogenesis (48), whereas monocyte CD36 blockade
372 prevents corneal lymphangiogenesis (49) suggesting a common mechanism in inflammatory
373 lymphangiogenesis induction. We hypothesise that the gross local dilation in parasitized skin
374 lymphangions impairs trafficking of solutes from proximal interstitial spaces during type-2
375 filarial inflammation. Lymphangion lumen dilation to the point of valve dysfunction has been
376 proposed as a mechanism for lymphostasis in post-surgical LE (50). In filarial hydrocele
377 pathology, gross ‘honeycomb’ dilation of the supra-testicular lymphatics correlates with
378 circulating VEGFA levels (15). As VEGFA and VEGFC both activate lymphatic endothelium
379 via VEGFR1/2 and VEGFR3, respectively, our data supports VEGFA/C-specific activation of
380 the superficial lymphatics during filarial type-2 inflammation, delivered by recruited CCR2+
381 monocytes and their subsequent differentiation into AAMϕ. However, we also identified
382 circulating and monocyte-specific production of other lymphangiogenic factors, namely sALK-
383 1 and prolactin, whilst another lymphangiogenic factor, Ang-2, which was IL-4R type-2
384 dependent in circulation, was not produced by the monocyte/macrophage lineage within

parasitized lymphatics. This suggests additional lymphangiogenic factors contribute to remodelling events during initiation of type-2 filarial inflammation within skin-draining lymphatics. The relative functional roles of these multiple growth factors need investigating to determine whether targeted antiangiogenics may be of therapeutic benefit in filarial LE.

In our human co-culture system, monocyte-differentiated Mϕ polarised with type-2 cytokines, resulted in a Mϕ phenotype able to induce LEC proliferation. However, live filarial larvae or their products could also induce a Mϕ phenotype without additional type-2 cytokine 'help'. Type-2 or filarial polarised monocyte-derived Mϕ *in vitro* produced increased secretions of VEGFA/C, follistatin and HGF. Filarial-specific activation of human $CD14^+$ monocytes has been prior demonstrated to induce pro-lymphangiogenic VEGFA secretions(9) . Thus, local 'patrolling' $CD14^+$ monocyte populations in the lymphatics may also be able to facilitate localised lymphatic dilations in the immediate vicinity of invading larvae in response to larval secretions. This may facilitate larval migrations through lymphatics and would occur prior to initiation of type-2 immunity, resulting in the recruitment of inflammatory monocytes, their differentiation into alternatively-activated Mϕ and resultant augmented and widespread lymphatic pathology.

Prior clinical research has promoted an anti-pathology role of six-week 200mg/day doxycycline treatment in ameliorating filarial LE pathologies (7, 16, 29, 51). Reduced circulating VEGFA/C were observed in these studies, strengthening a hypothesis that chronic lymphatic remodelling supports development and maintenance of filarial LE (7, 16, 29). The mechanism by which doxycycline mediates anti-morbidity effects in filariasis is difficult to determine in the clinic, due to its curative activity via targeting filarial *Wolbachia* (52), and its broad-spectrum antibiotic properties which reduce secondary skin bacterial infections and cellulitis complications (53). Further, *Wolbachia* can directly activate classical inflammatory processes upon liberation from filarial tissues (32) and have been identified as mediators of systemic adverse reactions in LF patients post-filaricidal treatment (54, 55). Therefore, *Wolbachia* may contribute to filarial LE via triggering classical inflammation (56) and

412 doxycycline may prevent this disease pathway. Upon characterising a type-2 inflammatory
413 response causal in inducing filarial lymphatic pathology, we exploited our model systems to
414 investigate the mode-of-action by which second-generation tetracyclines ameliorate filarial
415 lymphatic disease. First, we established both doxycycline and the related second-generation
416 tetracycline, minocycline, are directly anti-lymphangiogenic, blocking LEC proliferation to
417 VEGF stimuli. These data confirm earlier reports that doxycycline directly modifies VEGFC-
418 induced LEC proliferation by interrupting phosphorylation of phosphoinositide 3 kinase (PI3K),
419 alpha-serine/threonine protein kinase (AKT1) and endothelial nitric oxide synthase (eNOS)
420 signalling (57). We also determined the suppressive effect of doxycycline extends to inhibiting
421 LEC proliferation mediated by IL-4/13 or filarial-conditioned pro-angiogenic Mϕ. The anti-
422 angiogenic pharmacological activity of doxycycline or minocycline achieved *in vitro,* at
423 between 10-20 μM, was at or slightly higher than typical clinical peak-plasma concentrations.
424 However, concentrations of doxycycline, following 14-days dosing in the skin, are known to
425 accumulate three-fold more than measured in circulation (58). This suggests our effective
426 dose levels reflect local concentrations experienced within and surrounding superficial
427 lymphatics.
428 Anti-lymphangiogenic activities of doxycycline and minocycline were reproducible *in vivo,*
429 whereby oral dosing mice with human bioequivalent regimens (30), significantly reduced
430 magnitude of lymphatic remodelling and dysfunction induced by filarial infection. We
431 determined this anti-pathology mechanism was tetracycline-specific and unrelated to broad-
432 spectrum antibiotic or anti-*Wolbachia* efficacies. Lack of evidence for *Wolbachia* in lymphatic
433 pathology induction in our larval model probably reflects low *Wolbachia* titres in infectious
434 stage *B. malayi* and does not necessarily preclude a role for higher titres of *Wolbachia,*
435 liberated upon death of more mature filariae in parasitized lymphatics, augmenting LE
436 pathology development *in vivo*. The skewed, local type-2 inflammation observed in our mouse
437 model also reflects low *Wolbachia* exposure during initial immune priming, as we previously

demonstrated type-2 T cell polarisation by filarial extract becomes modified toward a mixed type-1 and type-2 T cell response by relative abundance of *Wolbachia* products (32).

Doxycycline modified the type-2 recruited monocyte / AAMϕ pathway of lymphatic pathology at multiple points *in vivo*. Thus, we demonstrate that doxycycline has wide-ranging immunosuppressive and anti-inflammatory activities in modulating filarial-induced type-2 inflammatory lymphangiogenesis. As doxycycline directly perturbed pro-lymphangiogenic Mϕ in response to type-2 or filarial-specific stimuli *in vitro,* this provides evidence of a specific targeted effect at the level of Mϕ. Doxycycline has previously shown to suppress IL-4/13 dependent alternative-activation of monocyte-derived Mϕ, with concomitant impairment in Mϕ-induced angiogenesis (59). The likely multi-faceted mechanisms by which second generation tetracyclines cause such wide-ranging anti-lymphangiogenic, anti-inflammatory and immuno-suppressive effects on mammalian cells to stymy filarial type-2 lymphatic pathogenesis require detailed further investigations. An assumed mode of doxycycline-mediated anti-angiogenic activity *in vivo* has been via targeted inhibition of matrix metalloproteinases (MMPs) to prevent extra-cellular matrix degradation necessary for neovascularisation (60, 61). One alternative, emerging mechanism is that doxycycline suppresses mammalian mitochondrial protein synthesis, thus shifting cellular metabolism toward glycolysis and slowing cell proliferative rate (62). Finally, a recent study demonstrates that calcium signalling is relevant in VEGFA-induced angiogenesis (63). Because doxycycline is a known calcium ion chelator, anti-angiogenic and more wide-spread anti-proliferative effects of the drug could be mediated by attenuating multiple calcium-dependent, second messenger signalling pathways. Certainly, the T cell anti-proliferative activity of doxycycline can be overcome by addition of exogenous calcium (64).

As with current indications in the treatment of rheumatoid arthritis or rosacea (65), we identify that the mode-of-action of second-generation tetracyclines in mediating anti-pathology efficacy in filariasis is via immuno-suppressant / anti-inflammatory activities. However, akin to the dual mode-of-action considered important in the treatment of acnes (65) we do not discount that second-generation tetracyclines are also beneficial to filarial LE patients by

resolving secondary bacterial infections, preventing ADLA episodes. Lipophilicity and dermal accumulation of second-generation tetracyclines may be important physiochemical features contributing to a 'long-tail' of anti-pathology activities in superficial lymphatics and local skin-draining lymph nodes. Because minocycline is a more lipophilic antibiotic compared with doxycycline (30), it may be a clinically superior treatment for filarial LE, warranting comparative clinical assessment, while newly approved formulations of minocycline (66) for the treatment of skin complaints warrants clinical assessment of anti-pathology effects in filarial LE patients. Because "sterile" post-surgical LE has been clearly linked with inflammation and leukotriene production (67), doxycycline may be of therapeutic benefit in the treatment of non-filarial LE of inflammatory origin, especially where cellulitis complications contribute to disease aetiology. Potential limitations of the deployment of oral second-generation tetracyclines as anti-morbidity therapy for filarial LE include the potential for gastrointestinal side effects, development of photosensitivity and contraindications during pregnancy and for young children. However, large scale implementation trials of doxycycline treatment as a cure for filariasis in over 13,000 African participants have determined >90% adherence to treatment and phase II trials have only reported infrequent and generally mild adverse effects during six-week therapy (68). Large-scale, multi-centre trials are currently commencing to evaluate doxycycline as an anti-morbidity therapy for filarial LE (69). Future clinical trials should also address dose duration and frequency, comparative efficacy of doxycycline versus minocycline and whether addition of affordable non-steroidal anti-inflammatory drugs, such as ketoprofen, which is currently undergoing clinical assessment for the treatment of post-surgery LE (70), may be of added benefit, including in contra-indicated groups.

In conclusion, our preclinical research establishes the mode-of-action of second-generation tetracyclines as anti-morbidity drugs in the therapy of filarial LE. These findings support the onward clinical evaluation of these affordable, readily available and safe treatments for LE of filarial origin and potentially for other LE associated with chronic inflammation.

Materials and Methods

Study design

Group sizes of animal experiments were determined using appropriate sample size calculations to power a study >80%. Data was pooled from repeat experiments where done. Mice were randomized into infection / intervention groups by ID number. Dosing and interventions were done in a non-blinded manner. Image-based readouts were blinded prior to analysis.

Experimental animals

Laboratory animals were maintained in SPF facilities at The Biomedical Services Unit, University of Liverpool. Mongolian gerbils, BALB/c/C57BL/6J IL-4rα$^{-/-}$, C57BL/6J Prox-1^{GFP}, and C57BL/6J TLR-6$^{-/-}$ mice were bred in house. Mongolian gerbils were originally purchased from Charles River, Europe. BALB/c IL-4rα$^{-/-}$ mice were originally purchased from Jackson Laboratories, USA. C57BL/6J IL-4rα$^{-/-}$ mice were originally gifted by Dr Cecile Benezech, Edinburgh University. FVB/N-Crl:CD1(ICR) Prox-1^{GFP} mice were provided by Professor Young-Kwon Hong, University of Southern California, before being back-crossed onto a C57BL/6J background for seven successive generations. C57BL/6J TLR-6$^{-/-}$ mice were originally gifted by Professor Shizuo Akira, Osaka University, Japan. Male BALB/c/C57BL/6J WT and CB.17 SCID mice were purchased from Charles River (Margate, UK). All mice were 6-12wk at the start of procedures. Gerbils were infected between 8-12wk old. Males were used in this study.

Parasite Life Cycle and Maintenance

B. malayi life cycle was maintained in mosquitoes and Mongolian gerbils as previously described (31). Briefly, microfilariae (mf) from >12wk infected gerbils were collected via peritoneal catheterisation. Purified and enumerated mf were mixed with heparinised human blood to 15–20,000 mf/ml and artificial membrane feeder (Hemotek) fed to female *Aedes*

aegypti mosquitoes. Following 14d, infective *B. malayi* L3 larvae (*Bm*L3) were collected from infected mosquitoes by crushing and Baermann's filtration.

Leg pathology model experimental infection

Mice were inoculated with 100 *Bm*L3 s.c., split between the top of left hind-foot and caudal to the left knee. Sham-infected mice received equal volumes of sterile RPMI1640.

Intravital Near-Infrared (NIR) Imaging of lymphatics

NIR imaging was adapted from techniques previously described (17). Briefly, anaesthetized mice were administered 20µl s.c. injections of 1mg/ml indocyanine green (ICG) (Sigma, Dorset UK) onto the top of left and right hind feet. Lymphatic drainage was monitored using a Photo Dynamic Eye (PDE) near infra-red (NIR) optical imaging device (Hamamatsu Photonics, Hertfordshire) to track NIR signal. Mice were imaged from 4 viewpoints: Dorsal, ventral, left and right. 720 x 480 at 60 fps movies (3 minutes per mouse) was recorded, using an EasyCap DC60 USB Video Capture Card Adapter (Softonic, Barcelona) that converted footage to ImageJ software (NIH, USA). 720x480 still images were used in downstream analysis. For more information see supplementary methods.

Evan's Blue dermal retention assay

A modified Miles Assay was utilised whereby mice were administered s.c injections of 10µl 1% Evan's Blue (Sigma, Dorset UK) w/v in sterile dPBS (Sigma, UK) on top of the infected hind-foot. After 20min, mice were euthanized and left hind-leg skin excised between the knee and ankle joint, transferred to 1ml of dPBS (Sigma, UK) and incubated 20min. Absorbance was read at 620nm on a plate spectrometer (VarioSkan, Bio-Rad).

Fluorescent microscopy

Skin samples from C57BL/6J Prox-1^{GFP} mice were dissected from areas of aberrant lymphatics (equivalent areas used in sham control mice). Lymphatic vessels were visualized using Prox-1^{GFP} epifluorescence under a fluorescent stereo-dissecting microscope, eGFP filter

(Leica Microsystems, Milton Keynes). Between 15- 30 images were taken per mouse, blinded, and lymphatic channels measured for aperture in ImageJ (NIH, USA). All image measurements were pooled/mouse to calculate average lymphatic widths.

*Bm*L3 were washed before incubation with 50μM Alexa Fluor™ 546 NHS Ester (Succinimidyl Ester) (Thermofisher, UK) in Fluorobrite DMEM (Thermofisher, UK) for 2h. C57BL/6J Prox-1^{GFP} transgenic mice were injected with 400 fluorescent *Bm*L3 as described above. After 3h and 1-6 dpi mice, areas of sub-cutaneous tissues where lymphatic remodeling occurs were imaged as above (DsRed and eGFP filters).

Lymphoid-, lymphatic,- splenic- and blood-single cell preparations

Cardiac blood was collected into heparinised tubes (Starstedt, Germany), centrifuged, plasma harvested and stored at -80ºC for downstream analysis. In blood immuno-phenotyping experiments, red blood cells were depleted using RBC lysis buffer (Biolegend, London), resuspended in dPBS (Sigma, Dorset) + 5% Foetal Bovine Serum (FBS) + 2mM EDTA (FACS buffer). Spleens or popliteal, iliac and sub-iliac lymph nodes with surrounding lymphatic collecting vessels were collected and a single cell suspension made by maceration through a 40μm cell sieve (Sigma, Dorset). Resultant cell suspensions were centrifuged, re-suspended in RPMI1640 or FACS buffer and enumerated.

Splenocyte and Lymph node cell recall assays

LN cells and Splenocytes were plated at $2.5x10^5$/well: splenocytes into previously coated 1.25μg/ml anti-CD3 wells followed by the addition of 2μg/ml anti-CD28 (Biolegend, UK). LN cells with no *ex vivo* stimulation. All cells were incubated for 72 hours at 37°C 5% CO_2 and subsequent supernatants frozen at -20°C.

Multiplex Protein Array Analysis

Multiplex immunoassays of 25 growth factors or 32 cytokine/chemokines (Mouse Angiogenesis/Growth Factor / Mouse Cytokine/Chemokine Magnetic Bead Panels, Merck)

were undertaken on plasma or re-stimulated splenocyte/lymph node cell cultures, following manufacturer's protocol. Plates were read on Bioplex 200 system (Bio-Rad, Watford, UK) and data analysed using Luminex XPONENT software (Luminexcorp, Netherlands).

Flow cytometry

Single cell suspensions were FcR-blocked before staining with viability dye and specific fluorescently labelled antibodies (Table S1), as previously described (22). For intracellular cytokine experiments, sdLN suspensions were stimulated for 5h in cell stimulation cocktail (ebioscience Hatfield), followed by CD4 and intracellular cytokine staining. Data acquisition was undertaken on a BD LSRII Flow cytometer (BD Biosciences, Berkshire, UK). Data was analysed using FlowJo software (BD Biosciences, UK) (Figure S4).

Fluorescent Antibody Cell Sorting (FACS) and cell secretion assays

Following surface staining, cell populations (Figure S4) were sorted using a Becton Dickinson FACsAria II (BD Biosciences, Berkshire, UK) to ≥95% purity into ice cold dPBS (Sigma, Dorset) + 40% FBS Serum + 2mM EDTA. Purified B and T-cells were plated at $1x10^6$ cells in 250µl, while monocytes and macrophages were plated at $2.5x10^5$ cells in 100µl into 96 well plates (Starlab, Milton Keynes). cells were incubated at 37ºC, 5% CO_2 for 72h and collected supernatants frozen at -80ºC.

Cell culture

Primary (adult)– Human Dermal Lymphatic Microvascular Endothelial Cells (HMVEC-dLyAd: LECs) and Human Dermal Microvascular Endothelial Cells – (HMVEC-dAd; BECs) were purchased from Lonza (Slough) and passaged in Endothelial Growth Medium-2 Bullet kit (EGM-2) (Lonza, Slough). THP-1 monocytes (ECACC, Public Health England) were passaged in RPMI 1640 (Sigma, Dorset) supplemented with: 10% FBS (Sigma, Dorset), Penicillin / Streptomycin 100 I.U./mL (Sigma, Dorset) and Amphotericin B 2.5mg/L (Sigma, Dorset). All cells were maintained at 37ºC, 5% CO_2.

592 *Brugia malayi L3 larval extract (BmL3E)*

593 Batches of 1000-2000 *B. malayi* L3 were washed, re-suspended in E-toxate water (Sigma,
594 Dorset) and extracts prepared as previously described (32), before storage at -20ºC.

595 *Macrophage/ LEC co-culture assay*

596 THP-1 monocytes were plated in 12-well trans-well inserts at $1x10^6$ cells/well and
597 differentiated into macrophages using 10ng/ml PMA (Sigma, Dorset) for 24h. Inserts were
598 washed and stimulated with indicated combinations of: 10µg/ml *Bm*L3E, 10 *Bm*L3, 10ng/ml
599 human rIL-4+rIL-13 or rIFNγ (all Peprotech), 10µM Doxycycline or 20% EGM-2 : 80%
600 endothelial basal media mix media only, for 48h. LECs were seeded separately on 12-well
601 plates at $4x10^4$ cells/well. Following 48h stimulation, inserts and LEC wells were washed
602 combined and incubated for 72h at 37ºC, 5% CO_2. LECs were enumerated following
603 harvesting from plates by microscopy.

604 *LEC/BEC proliferation assays*

605 LEC/BEC were plated at $2x10^5$cells/well into 96-well plates, stimulated with 2ng/ml VEGF165
606 (VEGF) (Lonza, Slough) with or without 10 or 20µM of either doxycycline or minocycline
607 (sigma, Dorset) and maintained at 37ºC, 5% CO_2, for 10d. Proliferation was quantified
608 longitudinally using the Incucyte live cell imaging platform with images taken hourly and results
609 plotted as fold change from confluence at hour 0.

610 *CCR2 and clodronate liposome monocyte/macrophage depletion experiments*

611 Following infection, mice were administered either: 20µg MC-21 rat anti-mouse CCR2
612 depleting antibody (Professor Matthias Mack, Rensburg University) (28) i.p., daily, or
613 2.5mg/ml clodronate liposome suspensions (Liposoma, Netherlands) s.c. at *Bm*L3 infection
614 sites every three days. Treatment was undertaken for 6d.

615 *Antibiotic screens*

616 Infected mice were randomized into groups and administered bi-daily: Doxycycline 40mg/kg,

Minocycline 25mg/kg, Amoxicillin 25mg/kg, Rifampicin 35mg/kg, Chloramphenicol 40mg/kg (all Sigma, UK) or ddH2O vehicle control via oral gavage for 14d.

Statistical Analysis

All continuous data was tested for normal distribution using the Kolmogorov-Smirnoff test. Where data was normally distributed, a two-tailed independent student's t-test (2 groups) or One-way ANOVA with a Tukey's post-hoc comparisons test (<2 groups) was used to test for significant differences. Where data was found to be not normally distributed, a log transformation was first attempted. If data remained non-parametric, a two-tailed Mann-Whitney U test (2 groups) or Kruskal-Wallis with Dunn's post-hoc multiple comparisons test (<2 groups) was utilised to test for significant differences between groups. The mean ± SEM are reported in all data unless otherwise stated. A P value <0.05 was considered significant. Significance is indicated as *=P<0.05, **=P<0.01, ***=P<0.001 ****=P<0.0001.

Study approval

All rodent experimental procedures were approved by the Animal Welfare Committee of University of Liverpool and The Animal Welfare and Ethics Review Board of Liverpool School of Tropical Medicine (LSTM) and carried out in accordance with The Use of Animals in Scientific Procedures Act (UK).

635 **Author Contributions**
636
637 Designed research studies: JFS, SDC, MJT, JDT

638 Conducted research: JFS, SDC, AEM, NP, JA, AS

639 Analysed data: JFS, SDC

640 Provided reagents and resources: SSM, MM, YKH, MJT, JDT

641 Wrote the manuscript: JFS, JDT

642

643 **References**

644 1. Rockson SG, Rivera KK. Estimating the Population Burden of Lymphedema. *Ann. N. Y.*
645 *Acad. Sci.* 2008;1131(1):147–154.

646 2. Grada AA, Phillips TJ. Lymphedema: Pathophysiology and clinical manifestations. *J. Am.*
647 *Acad. Dermatol.* 2017;77(6):1009–1020.

648 3. Mortimer PS, Rockson SG. New developments in clinical aspects of lymphatic disease. *J.*
649 *Clin. Invest.* 2014;124(3):915–21.

650 4. Ramaiah KD, Ottesen EA. Progress and Impact of 13 Years of the Global Programme to
651 Eliminate Lymphatic Filariasis on Reducing the Burden of Filarial Disease. *PLoS Negl. Trop.*
652 *Dis.* 2014;8(11):e3319.

653 5. Ton TGN, Mackenzie C, Molyneux DH. The burden of mental health in lymphatic filariasis.
654 *Infect. Dis. Poverty* 2015;4(1):34.

655 6. Addiss DG, Brady MA. Morbidity management in the Global Programme to Eliminate
656 Lymphatic Filariasis: a review of the scientific literature. *Filaria J.* 2007;6(1):2.

657 7. Mand S et al. Doxycycline Improves Filarial Lymphedema Independent of Active Filarial
658 Infection: A Randomized Controlled Trial. *Clin. Infect. Dis.* 2012;55(5):621–630.

659 8. Bennuru S, Nutman TB. Lymphatics in human lymphatic filariasis: in vitro models of
660 parasite-induced lymphatic remodeling. *Lymphat. Res. Biol.* 2009;7(4):215–219.

661 9. Weinkopff T, Mackenzie C, Eversole R, Lammie PJ. Filarial Excretory-Secretory Products
662 Induce Human Monocytes to Produce Lymphangiogenic Mediators. *PLoS Negl. Trop. Dis.*
663 2014;8(7):e2893.

664 10. Ah HS, Thompson PE. Brugia pahangi: infections and their effect on the lymphatic
665 system of Mongolian jirds (Meriones unguiculatus). *Exp Parasitol* 1973;34(3):393–411.

666 11. Vickery AC, Albertine KH, Nayar JK, Kwa BH. Histopathology of Brugia malayi-infected

667 nude mice after immune-reconstitution. *Acta Trop* 1991;49(1):45–55.

668 12. Jackson-Thompson BM et al. Brugia malayi infection in ferrets – A small mammal model
669 of lymphatic filariasis. *PLoS Negl. Trop. Dis.* 2018;12(3):e0006334.

670 13. Nelson FK, Greiner DL, Shultz LD, Rajan T V. The immunodeficient scid mouse as a
671 model for human lymphatic filariasis. *J Exp Med* 1991;173(3):659–663.

672 14. Freedman DO et al. Lymphoscintigraphic analysis of lymphatic abnormalities in
673 symptomatic and asymptomatic human filariasis. *J Infect Dis* 1994;170(4):927–933.

674 15. Debrah AY et al. Plasma vascular endothelial growth Factor-A (VEGF-A) and VEGF-A
675 gene polymorphism are associated with hydrocele development in lymphatic filariasis
676 [Internet]. *Am J Trop Med Hyg* 2007;77(4):601–608.

677 16. Debrah AY et al. Reduction in levels of plasma vascular endothelial growth factor-A and
678 improvement in hydrocele patients by targeting endosymbiotic Wolbachia sp. in Wuchereria
679 bancrofti with doxycycline. *Am J Trop Med Hyg* 2009;80(6):956–963.

680 17. Yamamoto T et al. Characteristic Indocyanine Green Lymphography Findings in Lower
681 Extremity Lymphedema: The Generation of a Novel Lymphedema Severity Staging System
682 Using Dermal Backflow Patterns. *Plast. Reconstr. Surg.* 2011;127(5):1979–1986.

683 18. Rajan T. et al. Brugian infections in the peritoneal cavities of laboratory mice: kinetics of
684 infection and cellular responses. *Exp. Parasitol.* 2002;100(4):235–247.

685 19. Coso S, Bovay E, Petrova T V. Pressing the right buttons: signaling in
686 lymphangiogenesis. *Blood* 2014;123(17):2614–2624.

687 20. Babu S, Nutman TB. Immunology of lymphatic filariasis. *Parasite Immunol.*
688 2014;36(8):338–346.

689 21. Babu S et al. Filarial lymphedema is characterized by antigen-specific Th1 and th17
690 proinflammatory responses and a lack of regulatory T cells. *PLoS Negl. Trop. Dis.*

691 2009;3(4):e420–e420.

692 22. Turner JD et al. Interleukin-4 activated macrophages mediate immunity to helminth
693 infection by sustaining CCR3-dependent eosinophilia. *PLOS Pathog.* 2018;

694 23. Shaw TN et al. Tissue-resident macrophages in the intestine are long lived and defined
695 by Tim-4 and CD4 expression. *J. Exp. Med.* 2018;215(6):1507–1518.

696 24. Mylonas KJ et al. The adult murine heart has a sparse, phagocytically active
697 macrophage population that expands through monocyte recruitment and adopts an “M2”
698 phenotype in response to Th2 immunologic challenge. *Immunobiology* 2015;220(7):924–
699 933.

700 25. Gundra UM et al. Alternatively activated macrophages derived from monocytes and
701 tissue macrophages are phenotypically and functionally distinct [Internet]. *Blood*
702 2014;123(20):e110–e122.

703 26. Thomas GD et al. The biology of nematode- and IL4Rα-dependent murine macrophage
704 polarization in vivo as defined by RNA-Seq and targeted lipidomics. *Blood*
705 2012;120(25):e93–e104.

706 27. Corliss BA, Azimi MS, Munson JM, Peirce SM, Murfee WL. Macrophages: An
707 Inflammatory Link Between Angiogenesis and Lymphangiogenesis. *Microcirculation*
708 2016;23(2):95–121.

709 28. Mack M et al. Expression and Characterization of the Chemokine Receptors CCR2 and
710 CCR5 in Mice. *J. Immunol.* 2001;166(7):4697–4704.

711 29. Debrah AY et al. Doxycycline reduces plasma VEGF-C/sVEGFR-3 and improves
712 pathology in lymphatic filariasis. *PLoS Pathog.* 2006;2(9):e92–e92.

713 30. Sharma R et al. Minocycline as a re-purposed anti-Wolbachia macrofilaricide: superiority
714 compared with doxycycline regimens in a murine infection model of human lymphatic
715 filariasis. *Sci. Rep.* 2016;6(1):23458.

716 31. Halliday A et al. A murine macrofilaricide pre-clinical screening model for onchocerciasis
717 and lymphatic filariasis. *Parasit. Vectors* 2014;7(1):472.

718 32. Turner JD et al. Wolbachia lipoprotein stimulates innate and adaptive immunity through
719 Toll-like receptors 2 and 6 to induce disease manifestations of filariasis. *J. Biol. Chem.*
720 2009;284(33):22364–78.

721 33. Aljayyoussi G et al. Short-Course, High-Dose Rifampicin Achieves Wolbachia Depletion
722 Predictive of Curative Outcomes in Preclinical Models of Lymphatic Filariasis and
723 Onchocerciasis. *Sci. Rep.* 2017;7(1):210.

724 34. Johnston KL et al. Repurposing of approved drugs from the human pharmacopoeia to
725 target Wolbachia endosymbionts of onchocerciasis and lymphatic filariasis. *Int. J. Parasitol.*
726 *Drugs Drug Resist.* 2014;4(3):278–286.

727 35. Bennuru S, Maldarelli G, Kumaraswami V, Klion AD, Nutman TB. Elevated levels of
728 plasma angiogenic factors are associated with human lymphatic filarial infections. *Am. J.*
729 *Trop. Med. Hyg.* 2010;83(4):884–890.

730 36. Satapathy AK et al. Human bancroftian filariasis: immunological markers of morbidity
731 and infection. *Microbes Infect.* 2006;8(9–10):2414–2423.

732 37. Kar SK et al. Lymphatic pathology in asymptomatic and symptomatic children with
733 Wuchereria bancrofti infection in children from Odisha, India and its reversal with DEC and
734 albendazole treatment doi:10.1371/journal.pntd.0005631

735 38. Howells RE, Devaney E, Smith G, Hedges T. The susceptibility of BALB/C and other
736 inbred mouse strains to Brugia pahangi. *Acta Trop.* 1983;40(4):341–50.

737 39. Pionnier N et al. Eosinophil-Mediated Immune Control of Adult Filarial Nematode
738 Infection Can Proceed in the Absence of IL-4 Receptor Signaling. *J. Immunol.*
739 2020;205(3):731–740.

740 40. Ewert A, Folse D. Animal model of human disease. Lymphatic filariasis. *Am J Pathol*

741 1984;115(1):135–137.

742 41. Snowden KF, Hammerberg B. The lymphatic pathology of chronic brugia pahangi
743 infection in the dog. *Trans. R. Soc. Trop. Med. Hyg.* 1989;83(5):670–678.

744 42. Zampell JC et al. CD4+ Cells Regulate Fibrosis and Lymphangiogenesis in Response to
745 Lymphatic Fluid Stasis. *PLoS One* 2012;7(11):e49940.

746 43. Avraham T et al. Th2 differentiation is necessary for soft tissue fibrosis and lymphatic
747 dysfunction resulting from lymphedema. *FASEB J.* 2013;27(3):1114–1126.

748 44. Jenkins SJ et al. Local macrophage proliferation, rather than recruitment from the blood,
749 is a signature of T H2 inflammation. *Science.* 2011;332(6035):1284–1288.

750 45. Riabov V et al. Role of tumor associated macrophages in tumor angiogenesis and
751 lymphangiogenesis. *Front. Physiol.* 2014;5:75.

752 46. Babu S, Kumaraswami V, Nutman TBB. Alternatively Activated and Immunoregulatory
753 Monocytes in Human Filarial Infections. *J. Infect. Dis.* 2009;199(12):1827–1837.

754 47. Babu S et al. Toll-Like Receptor- and Filarial Antigen-Mediated, Mitogen-Activated
755 Protein Kinase- and NF-κB-Dependent Regulation of Angiogenic Growth Factors in Filarial
756 Lymphatic Pathology. *Infect. Immun.* 2012;80(7):2509–2518.

757 48. Becker F et al. A critical role for monocytes/macrophages during intestinal inflammation-
758 associated lymphangiogenesis. *Inflamm. Bowel Dis.* 2016;22(6):1326–1345.

759 49. Cursiefen C et al. Thrombospondin 1 inhibits inflammatory lymphangiogenesis by CD36
760 ligation on monocytes. *J. Exp. Med.* 2011;208(5):1083–1092.

761 50. Jiang X, Nicolls MR, Tian W, Rockson SG. Lymphatic Dysfunction, Leukotrienes, and
762 Lymphedem. *Annu. Rev. Physiol.* 2018;80(1):49–70.

763 51. Mand S et al. Macrofilaricidal activity and amelioration of lymphatic pathology in
764 bancroftian filariasis after 3 weeks of doxycycline followed by single-dose

765 diethylcarbamazine. *Am. J. Trop. Med. Hyg.* 2009;81(4):702–711.

766 52. Taylor MJ et al. Macrofilaricidal activity after doxycycline treatment of Wuchereria
767 bancrofti: A double-blind, randomised placebo-controlled trial. *Lancet* 2005;365(9477):2116–
768 2121.

769 53. Ruhe JJ, Menon A. Tetracyclines as an oral treatment option for patients with community
770 onset skin and soft tissue infections caused by methicillin-resistant Staphylococcus aureus.
771 *Antimicrob. Agents Chemother.* 2007;51(9):3298–3303.

772 54. Andersen BJ et al. Systems analysis-based assessment of post-treatment adverse
773 events in lymphatic filariasis. *PLoS Negl. Trop. Dis.* 2019;13(9):e0007697.

774 55. Turner JD et al. A Randomized, Double-Blind Clinical Trial of a 3-Week Course of
775 Doxycycline plus Albendazole and Ivermectin for the Treatment of Wuchereria bancrofti
776 Infection. *Clin. Infect. Dis.* 2006;42(8):1081–1089.

777 56. Pfarr KM, Debrah AY, Specht S, Hoerauf A. Filariasis and lymphoedema. *Parasite*
778 *Immunol.* 2009;31(11):664–672.

779 57. Han L et al. Doxycycline Inhibits Inflammation-Induced Lymphangiogenesis in Mouse
780 Cornea by Multiple Mechanisms. *PLoS One* 2014;9(9):e108931.

781 58. Pal A et al. Target site pharmacokinetics of doxycycline for rosacea in healthy volunteers
782 is independent of the food effect. *Br. J. Clin. Pharmacol.* 2018;84(11):2625–2633.

783 59. He L, Marneros AG. Doxycycline inhibits polarization of macrophages to the
784 proangiogenic M2-type and subsequent neovascularization. *J. Biol. Chem.*
785 2014;289(12):8019–8028.

786 60. Samtani S, Amaral J, Campos MM, Fariss RN, Becerra SP. Doxycycline-mediated
787 inhibition of choroidal neovascularization. *Investig. Ophthalmol. Vis. Sci.* 2009;50(11):5098–
788 5106.

789 61. Liu J, Khalil RA. Matrix Metalloproteinase Inhibitors as Investigational and Therapeutic
790 Tools in Unrestrained Tissue Remodeling and Pathological Disorders [Internet]. *Prog. Mol.*
791 *Biol. Transl. Sci.* 2017;148:355–420.

792 62. Ahler E et al. Doxycycline Alters Metabolism and Proliferation of Human Cell Lines
793 [Internet]. *PLoS One* 2013;8(5):e64561.

794 63. Savage AM et al. tmem33 is essential for VEGF-mediated endothelial calcium
795 oscillations and angiogenesis. *Nat. Commun.* 2019;10(1):1–15.

796 64. Kloppenburg M et al. The influence of tetracyclines on T cell activation. *Clin. Exp.*
797 *Immunol.* 2008;102(3):635–641.

798 65. Sapadin AN, Fleischmajer R. Tetracyclines: Nonantibiotic properties and their clinical
799 implications. *J. Am. Acad. Dermatol.* 2006;54(2):258–265.

800 66. Bonati LM, Dover JS. Treating Acne With Topical Antibiotics: Current Obstacles and the
801 Introduction of Topical Minocycline as a New Treatment Option. *J. Drugs Dermatol.*
802 2019;18(3):240–244.

803 67. Tian W et al. Leukotriene B_4 antagonism ameliorates experimental lymphedema. *Sci.*
804 *Transl. Med.* 2017;9(389):eaal3920.

805 68. Wanji S et al. Community-directed delivery of doxycycline for the treatment of
806 onchocerciasis in areas of co-endemicity with loiasis in Cameroon. *Parasit. Vectors*
807 2009;2(1):39.

808 69. Horton J et al. The design and development of a multicentric protocol to investigate the
809 impact of adjunctive doxycycline on the management of peripheral lymphoedema caused by
810 lymphatic filariasis and podoconiosis. *Parasit. Vectors* 2020;13(1):155.

811 70. Rockson SG et al. Pilot studies demonstrate the potential benefits of antiinflammatory
812 therapy in human lymphedema. *JCI Insight* 2018;3(20).

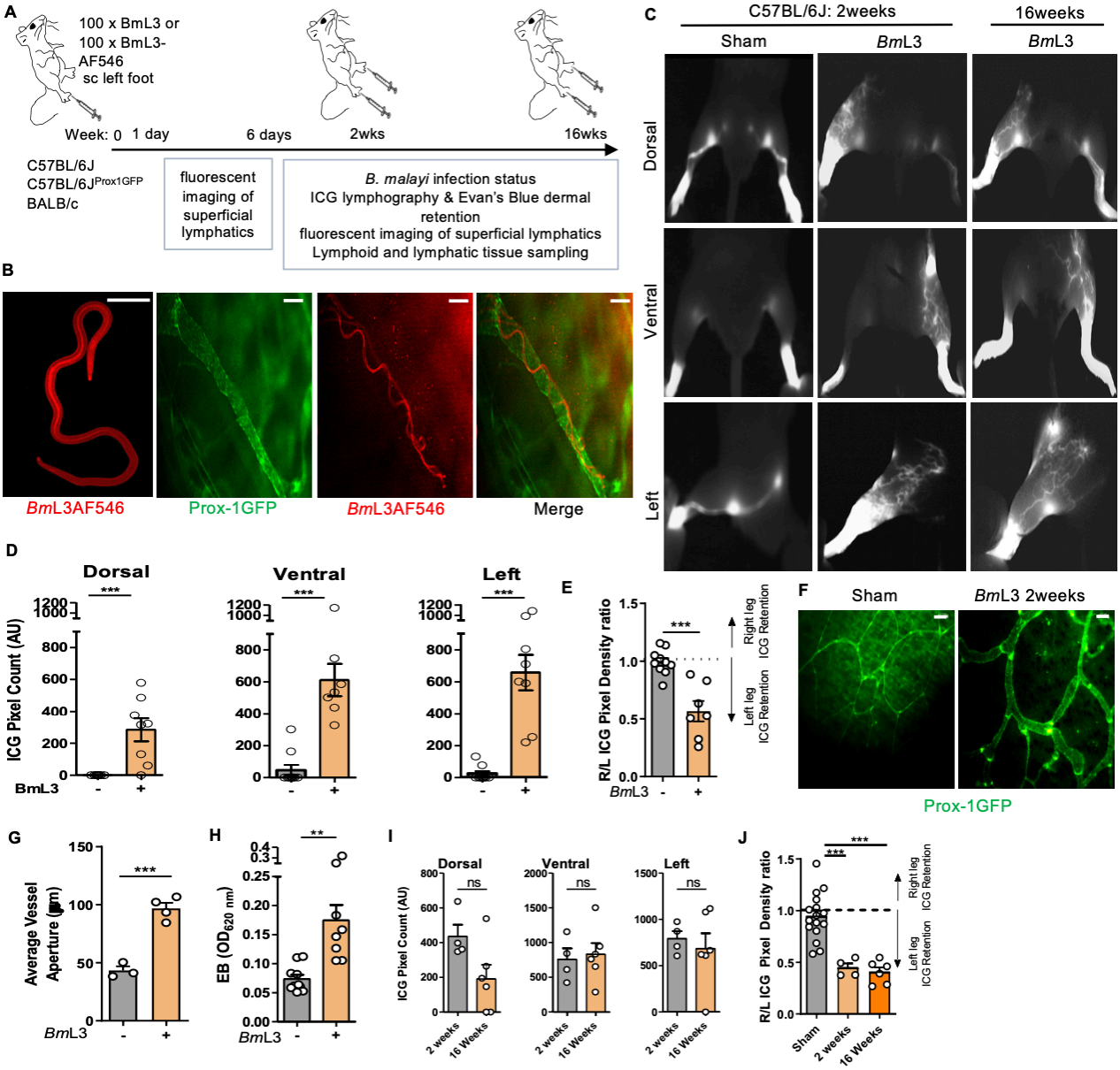
A
100 x BmL3 or
100 x BmL3-AF546
sc left foot
Week: 0
1 day
6 days
2wks
16wks
C57BL/6J
C57BL/6J Prox1GFP
BALB/c
fluorescent imaging of superficial lymphatics
B. malayi infection status
ICG lymphography & Evan's Blue dermal retention
fluorescent imaging of superficial lymphatics
Lymphoid and lymphatic tissue sampling
B
BmL3AF546
Prox-1GFP
BmL3AF546
Merge
C
C57BL/6J: 2weeks
16weeks
Sham
BmL3
BmL3
Dorsal
Ventral
Left
D
Dorsal
Ventral
Left
ICG Pixel Count (AU)
BmL3
E
R/L ICG Pixel Density ratio
Right leg ICG Retention
Left leg ICG Retention
F
Sham
BmL3 2weeks
Prox-1GFP
G
Average Vessel Aperture (μm)
H
EB (OD620 nm)
I
Dorsal
Ventral
Left
ICG Pixel Count (AU)
ns
2 weeks
16 Weeks
J
R/L ICG Pixel Density ratio
Sham
2 weeks
16 Weeks

Figure 1 *Filarial lymphatic infection induces persistent lymphatic pathology*

A) Schematic of hind-limb filarial infection model **B)** Representative images of *in vitro* (left panel) or intra-lymphatic AF456-labelled *Bm*L3 larvae in C57BL/6J Prox-1^{GFP} mice, 1dpi. **C)** Representative PDE intra-vital images of sham-infected and *Bm*L3-infected C57BL/6J mice,14dpi **D)** Quantified aberrant lymphatics and **E)** Quantified hind-limb ICG dye retention from PDE imaging expressed as a ratio of fluorescence in the right 'R' (uninfected) : left 'L' (infected) hind-limb (n=10 sham, n=8 *Bm*L3). **F)** Representative epifluorescence micrographs of dermal lymphatics and **G)** average dermal lymphatic vessel aperture in Prox-1^{GFP} mice 14dpi, (n=3 Sham, n=4 BmL3). Scale bars=200μm. **H)** Evan's Blue left hind-limb dermal retention (n=9 sham, n=8 *Bm*L3). **I)** aberrant lymphatics and **J)** hind-limb ICG retention comparing 2- and 16-week old infections (n=15 sham, n=4 *Bm*L3 2wpi, n=4 16 wpi). Histograms are mean±SEM **(D-J).** Data is pooled from 3 individual experiments (**D-E**), 2 individual experiments (**J**) or 1 individual experiment (**G, I-J**). Significance is indicated as **=P<0.01, ***=P<0.001 derived from a one-way ANOVA with Tukey's multiple comparisons post-hoc test (**J**) or two-tailed Student's t-test (**D-I**).

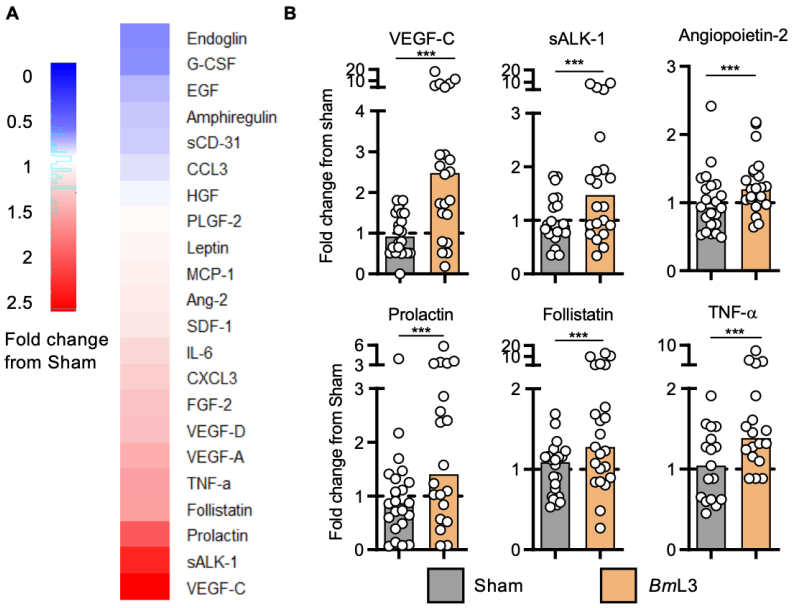
A
0
0.5
1
1.5
2
2.5
Fold change from Sham
Endoglin
G-CSF
EGF
Amphiregulin
sCD-31
CCL3
HGF
PLGF-2
Leptin
MCP-1
Ang-2
SDF-1
IL-6
CXCL3
FGF-2
VEGF-D
VEGF-A
TNF-a
Follistatin
Prolactin
sALK-1
VEGF-C
B
VEGF-C
sALK-1
Angiopoietin-2
Prolactin
Follistatin
TNF-α
***
Fold change from sham
Sham
BmL3

833

834

Figure 2 *filarial infection induces increases in circulating lymphangiogenic molecules*

A) circulating levels of lymphangiogenic molecules. Heatmap plots median fold-change in analyte from sham-infected mouse group; red = fold-increase from sham-infected, blue = fold-decrease (n=21 Sham; n=22 *Bm*L3) **B)** circulating lymphangiogenic molecule concentrations from **(A)** for analytes achieving statistical significance. Histograms are medians. Data is pooled from 4 individual experiments. Significance is indicated as ***=P<0.001 derived from a Mann-Whitney test.

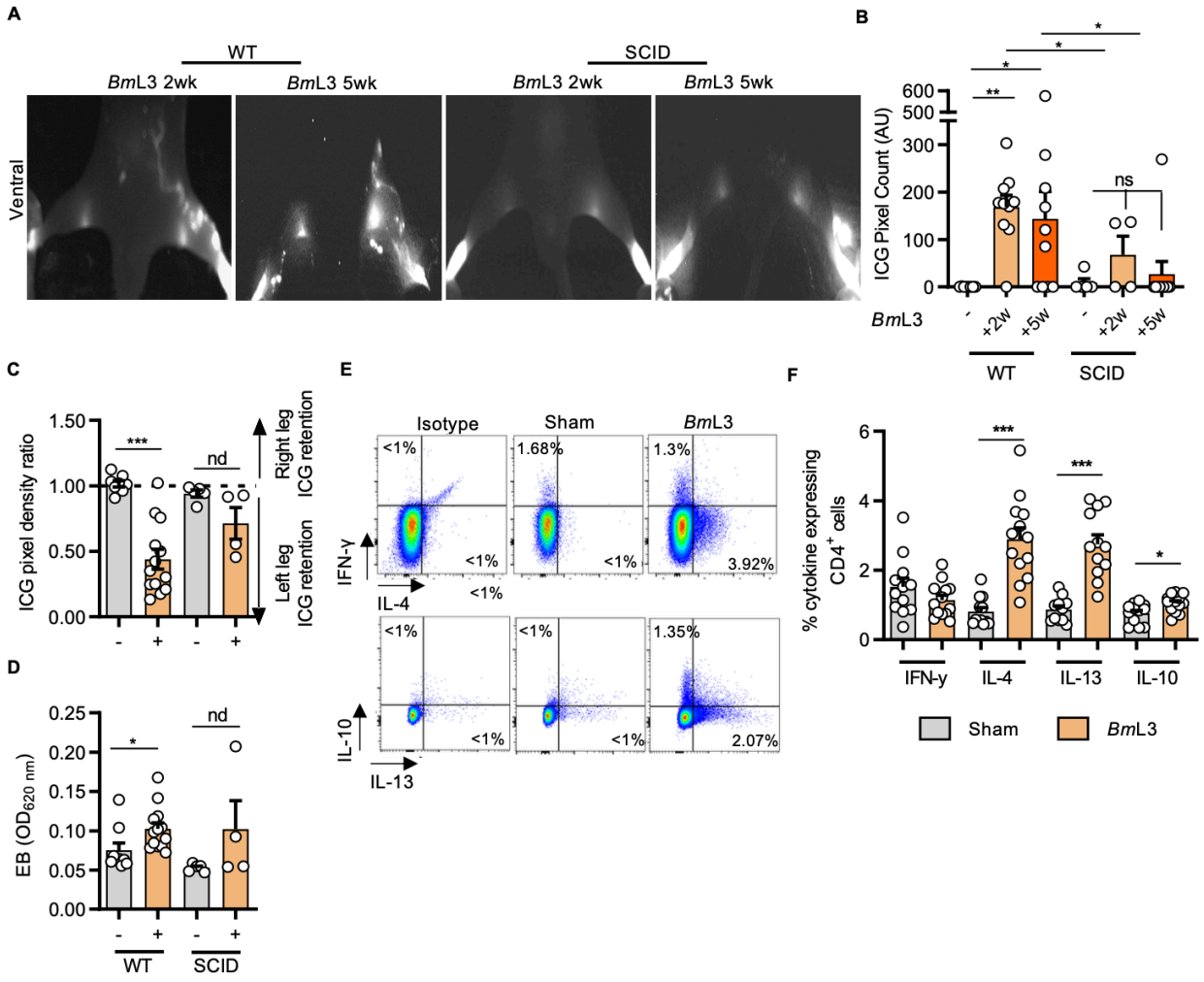
A
WT
SCID
BmL3 2wk
BmL3 5wk
BmL3 2wk
BmL3 5wk
Ventral
B
ICG Pixel Count (AU)
600
500
300
200
100
0
*
*
*
**
ns
BmL3
-
+2w
+5w
-
+2w
+5w
WT
SCID
C
ICG pixel density ratio
1.50
1.00
0.50
0.00
***
nd
Right leg ICG retention
Left leg ICG retention
-
+
-
+
D
EB (OD620 nm)
0.25
0.20
0.15
0.10
0.05
0.00
*
nd
-
+
-
+
WT
SCID
E
Isotype
Sham
BmL3
IFN-γ
IL-4
IL-10
IL-13
<1%
1.68%
1.3%
3.92%
1.35%
2.07%
F
% cytokine expressing CD4+ cells
6
4
2
0
***
***
*
IFN-γ
IL-4
IL-13
IL-10
Sham
BmL3

843

844

845

Figure 3 *filarial-associated lymphatic pathology is dependent on type-2 adaptive immunity* **A)** Representative PDE intravital images and **B)** aberrant lymphatic quantification of BALB/c wild-type (WT) and SCID mice at 2- and 5wpi (n=8 WT sham, n=10 WT *Bm*L3 +2wpi and 5wpi, n=5 SCID sham, n=4 SCID *Bm*L3 2wpi, n=10 SCID *Bm*L3 5wpi) **C)** hind-limb ICG dye retention and **D)** Evan's Blue left hind-limb dermal retention in WT and SCID mice, 14dpi (n=7 WT sham, n=14 WT *Bm*L3, n=5 SCID sham, n=4 SCID *Bm*L3) **E)** Representative flow cytometry plots and **F)** quantified cytokine production within skin-draining lymph node $CD4^+$ T-cells from C57BL/6J mice, 14dpi (n=12 Sham, n=13 *Bm*L3). Data is cytokine expressing cells as a proportion of total $CD4^+$ T cells. Histograms are mean±SEM. Data is pooled from 2 individual experiments (**B,D,F**) or a single experiment (**D**). Significance is indicated as *=P<0.05, **=P<0.01, ***=P<0.001, one-way ANOVA with Tukey's multiple comparisons post-hoc test between marked groups.

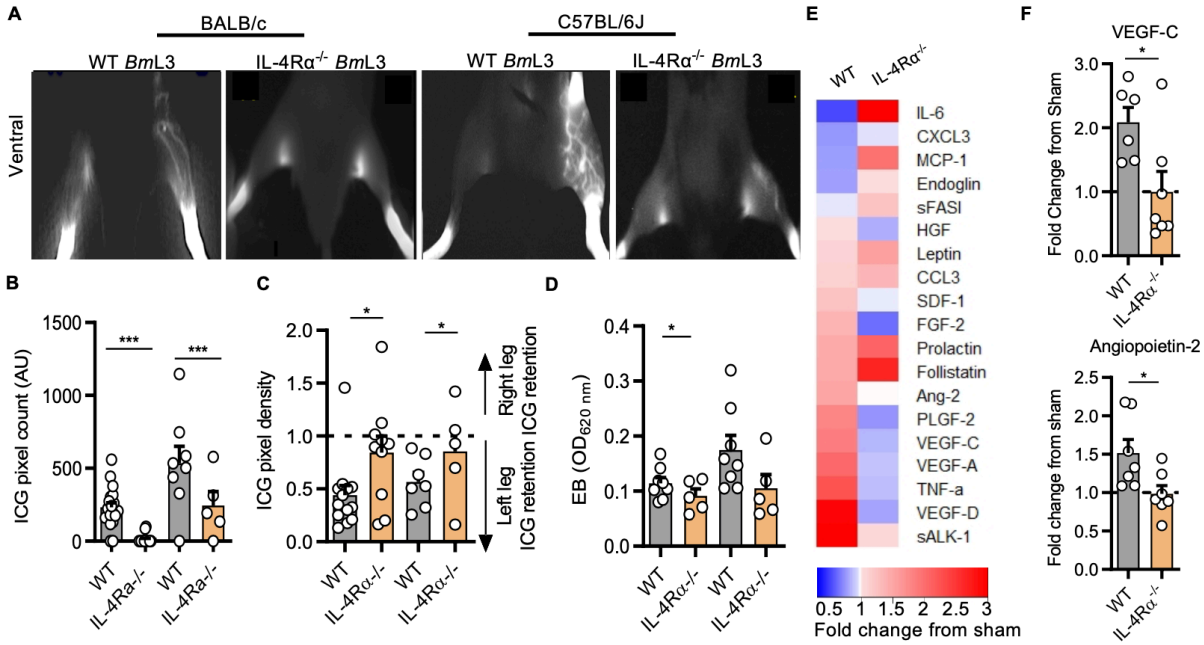
A
BALB/c
C57BL/6J
WT BmL3
IL-4Rα-/- BmL3
WT BmL3
IL-4Rα-/- BmL3
Ventral
B
ICG pixel count (AU)
1500
1000
500
0
***
***
WT
IL-4Rα-/-
WT
IL-4Rα-/-
C
ICG pixel density
2.0
1.5
1.0
0.5
0.0
*
*
Right leg
Left leg
ICG retention
ICG retention
WT
IL-4Rα-/-
WT
IL-4Rα-/-
D
EB (OD620 nm)
0.4
0.3
0.2
0.1
0.0
*
WT
IL-4Rα-/-
WT
IL-4Rα-/-
E
WT
IL-4Rα-/-
IL-6
CXCL3
MCP-1
Endoglin
sFASI
HGF
Leptin
CCL3
SDF-1
FGF-2
Prolactin
Follistatin
Ang-2
PLGF-2
VEGF-C
VEGF-A
TNF-a
VEGF-D
sALK-1
0.5 1 1.5 2 2.5 3
Fold change from sham
F
VEGF-C
Fold Change from Sham
3.0
2.0
1.0
0.0
*
WT
IL-4Rα-/-
Angiopoietin-2
Fold change from sham
2.5
2.0
1.5
1.0
0.5
0.0
*
WT
IL-4Rα-/-

860

861

862

Figure 4 *filarial-associated lymphatic pathology is dependent IL-4 receptor immune responses* **A)** Representative images, **B)** quantified aberrant lymphatics and **C)** quantified hind-limb ICG dye retention in WT and IL-4Rα$^{-/-}$ BALB/c and C57BL/6J mice, 14dpi (n=20 BALB/c WT sham, n=21 BALB/c WT *Bm*L3, n=8 IL-4Rα$^{-/-}$ BALB/c sham, n=15 IL-4Rα$^{-/-}$ BALB/c *Bm*L3, n=10 WT C57BL/6J sham, n=10 WT C57BL/6J *Bm*L3, n=5 IL-4Rα$^{-/-}$ sham and IL-4Rα$^{-/-}$ *Bm*L3). **D)** Evan's Blue left hind-limb dermal retention in WT and IL-4Rα$^{-/-}$ mice, 14dpi (n=8 BALB/c WT *Bm*L3, n=5 IL-4Rα$^{-/-}$ BALB/c *Bm*L3, n=8 WT C57BL/6J *Bm*L3, n=5 IL-4Rα$^{-/-}$ sham & IL-4Rα$^{-/-}$ *Bm*L3) **E)** Circulating levels of lymphangiogenic molecules between C57BL/6J WT and IL-4Rα$^{-/-}$ BmL3 infected mice, 14dpi. Heat-map plots median fold-change in analyte from sham-infected mouse group; red = fold-increase from sham-infected, blue = fold-decrease (n=6 WT *Bm*L3, n=7 IL-4Rα$^{-/-}$ *Bm*L3). **F)** Plots of lymphangiogenic analytes achieving statistical significance. Histograms are mean±SEM. Data is pooled from 2-3 individual experiments; Significance is indicated as *=P<0.05, ***=P<0.001, one-way ANOVA with Tukey's multiple comparisons post-hoc test (**B-D**) or two-tailed Student's t-test between marked groups **(F).**

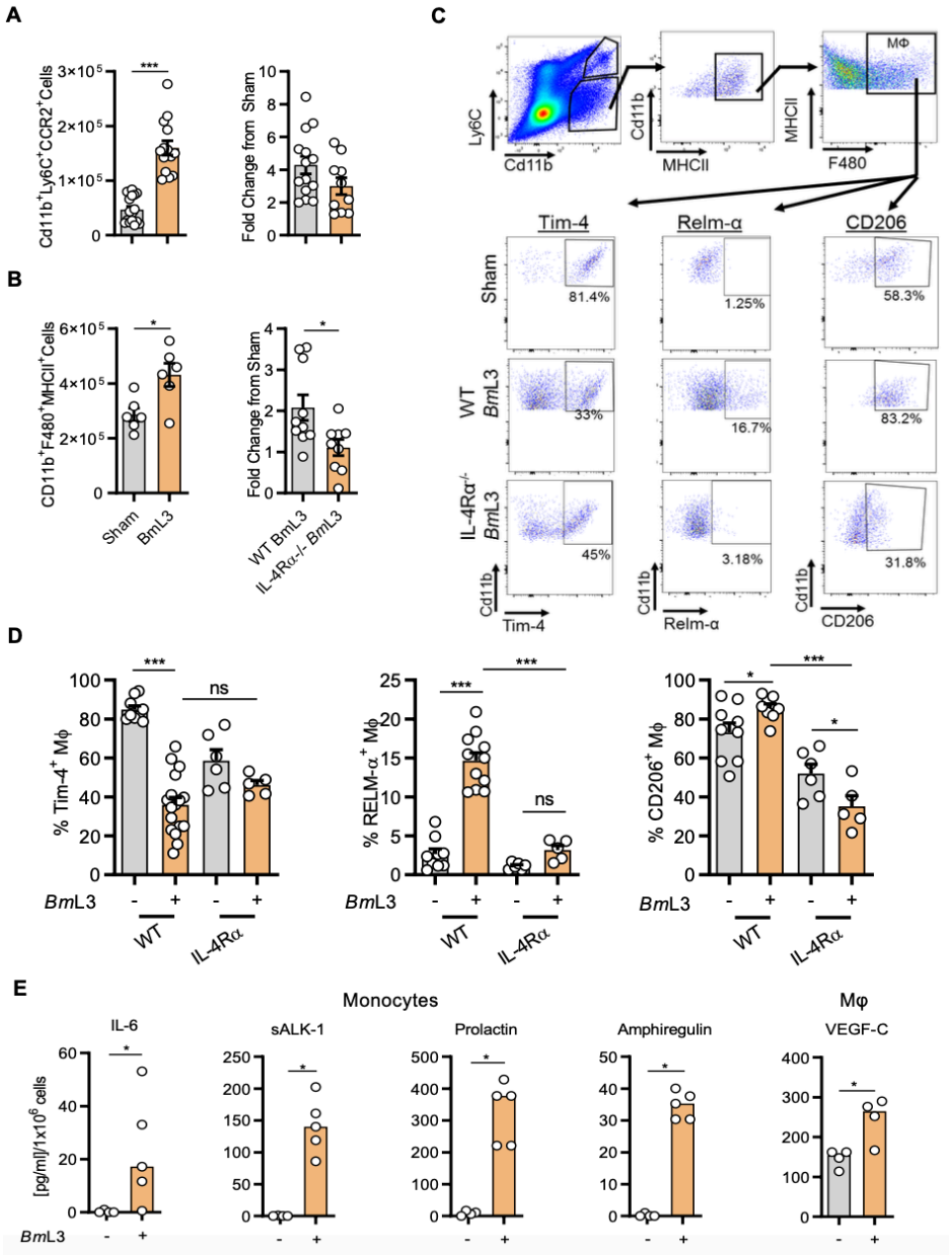
A
B
C
D
E
Monocytes
Mφ
Tim-4
Relm-α
CD206
Sham
WT BmL3
IL-4Rα-/- BmL3
BmL3
WT
IL-4Rα
IL-6
sALK-1
Prolactin
Amphiregulin
VEGF-C
[pg/ml]/1x10^6 cells

Figure 5 *BmL3 infection drives lymphatic monocyte recruitment and expansion of alternatively activated, pro-lymphangiogenic macrophages*

A) Numbers of $CD11b^{+}Ly6C^{+}CCR2^{+}$ inflammatory monocytes (n=16 Sham, n=14 WT *Bm*L3, n=10 IL-4Rα$^{-/-}$ *Bm*L3) or **B)** $Cd11b^{+}F480^{+}MHCII^{+}$ MΦ (n=6 Sham, n=10 WT *Bm*L3; n=9 IL-4Rα$^{-/-}$ *Bm*L3) derived from sdLNs and major lymphatic channels in C57BL/6J mice, 14dpi. Data is total cell numbers or fold-change from relevant sham controls **C)** Representative flow plots of lymphatic MΦ phenotyping in sham and *Bm*L3 infected mice. Percentages are proportions of total $CD11b^{+}F480^{+}MHCII^{+}$ MΦ. **D)** $CD206^{+}$, RELM-α^{+} and Tim-4^{+} MΦ expression in WT and IL-4Rα$^{-/-}$ sham and *Bm*L3 infected mice (n=9 WT Sham, n=9-17 WT *Bm*L3, n=6 IL-4Rα$^{-/-}$ sham, n=5 IL-4Rα$^{-/-}$ *Bm*L3). E) Significant changes in specific lymphangiogenic molecules secreted following 72-hour incubation *ex vivo* of FACS sorted lymphatic monocytes or MΦ derived from sham or *Bm*L3 infected mice. Secretion is normalised to analyte concentration/1x10^{6} cells (n=4 Sham, n=5 BmL3). Data is pooled from (2-3 individual experiments). Histograms are mean ±SEM (**A-D**) or median (**E**). Significance is indicated as *=P<0.05, **=P<0.01, ***=P<0.001, ns= not significant, derived from a two-tailed student t-test (**A-B**), a one-way ANOVA with Tukey's multiple comparisons post-hoc test **D**) or a Mann Whitney Test (**E**).

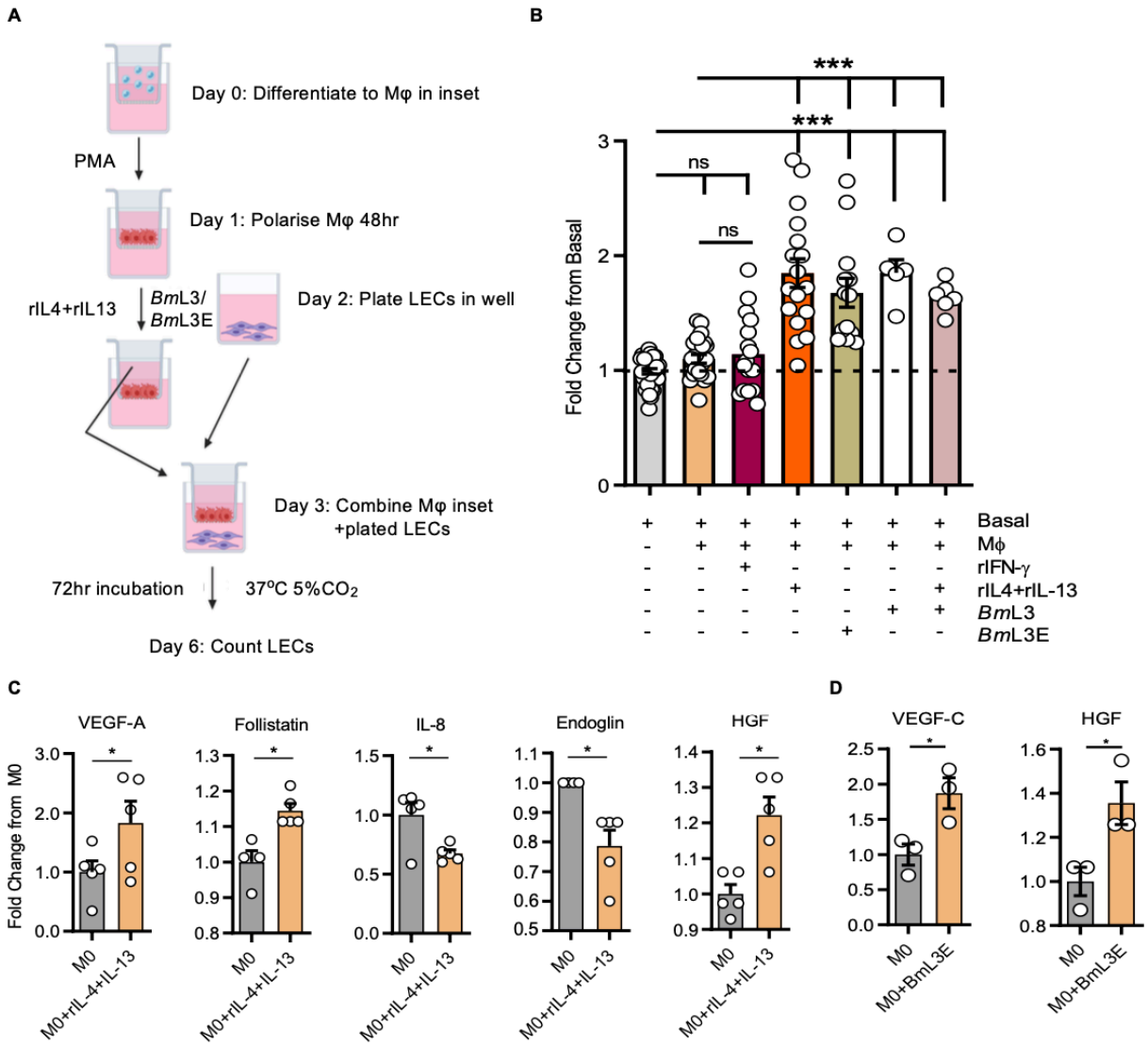
A
Day 0: Differentiate to Mφ in inset
PMA
Day 1: Polarise Mφ 48hr
rIL4+rIL13
BmL3/
BmL3E
Day 2: Plate LECs in well
Day 3: Combine Mφ inset
+plated LECs
72hr incubation
37°C 5%CO2
Day 6: Count LECs
B
***
***
ns
ns
Fold Change from Basal
Basal
Mϕ
rIFN-γ
rIL4+rIL-13
BmL3
BmL3E
C
VEGF-A
Follistatin
IL-8
Endoglin
HGF
Fold Change from M0
M0
M0+rIL-4+IL-13
D
VEGF-C
HGF
M0
M0+BmL3E

Figure 6 *Human monocyte-derived MΦ conditioned with rIL-4 + rIL-13 and/or filarial L3 results in a lymphangiogenic phenotype that induces proliferation of lymphatic endothelium.*

A) Schematic of *in vitro* human dermal lymphatic endothelial cells (LEC) co-cultured with pre-conditioned human monocyte-derived Mϕ. LEC proliferation was quantified 72-hour post addition of Mϕ co-cultures. **B)** LEC proliferation following monocyte derived MΦ co-cultures conditioned with: recombinant IL-4 + IL-13 (rIL-4+rIL-13), live *Bm*L3 (*Bm*L3), *Bm*L3 larval extract (*Bm*L3E), rIL+4+rIL-13+*Bm*L3 or unconditioned MΦ, expressed as fold-changes from mean basal LEC enumerations **C)** Concentrations of lymphangiogenic molecules 72 hours following Mϕ culture in the absence or presence of rIL-4+rIL-13 or **D**) *Bm*L3E (Mϕ+*Bm*L3E), expressed as fold-changes from mean unstimulated Mϕ levels (M0). Histograms are mean ±SEM. Data is pooled from 3 individual experiments (**A-B**) or a single experiment (**C+D**). Significance is indicated as *=P<0.05, **=P<0.01, ***=P<0.001, derived from a one-way ANOVA with Tukey's multiple comparisons post-hoc test (**B**) or a two-tailed Student's t-test between indicated groups (**C+D**).

916

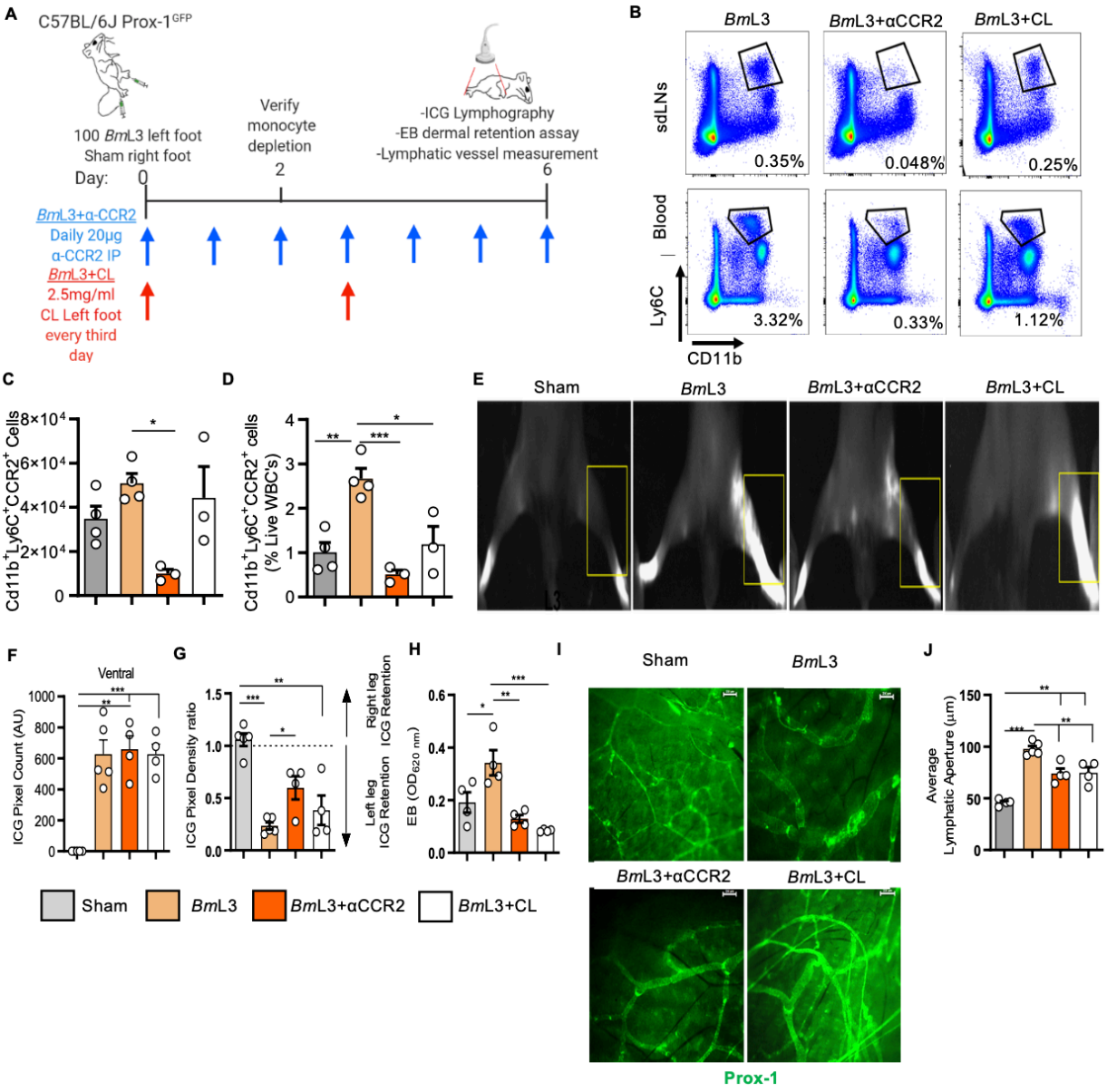
A
C57BL/6J Prox-1GFP
100 BmL3 left foot
Sham right foot
Day: 0
Verify monocyte depletion
2
-ICG Lymphography
-EB dermal retention assay
-Lymphatic vessel measurement
6
BmL3+α-CCR2
Daily 20µg α-CCR2 IP
BmL3+CL
2.5mg/ml CL Left foot every third day
B
BmL3
BmL3+αCCR2
BmL3+CL
sdLNs
Blood
Ly6C
CD11b
0.35%
0.048%
0.25%
3.32%
0.33%
1.12%
C
Cd11b+Ly6C+CCR2+ Cells
D
Cd11b+Ly6C+CCR2+ cells (% Live WBC's)
E
Sham
BmL3
BmL3+αCCR2
BmL3+CL
F
Ventral
ICG Pixel Count (AU)
G
ICG Pixel Density ratio
Left leg ICG Retention
Right leg ICG Retention
H
EB (OD620 nm)
I
Sham
BmL3
BmL3+αCCR2
BmL3+CL
Prox-1
J
Average Lymphatic Aperture (µm)
Sham
BmL3
BmL3+αCCR2
BmL3+CL

917

Figure 7 *Depletion of CCR2^{+} monocytes or phagocytes significantly ameliorates filarial-induced lymphatic insufficiency.*

A) Schematic of CCR2^{+} monocyte and phagocyte depletion regimens in *Bm*L3-infected C57BL/6J Prox-1^{GFP} mice **B)** Representative flow cytometry plots from *Bm*L3 infected, *Bm*L3 infected and either: treated with anti-CCR2 ablating antibody (*Bm*L3+αCCR2) or clodronate (*Bm*L3+CL), 2dpi. Percentages are CD11b^{+}Ly6C^{+} cells as a proportion of live cells. **C)** CD11b^{+}Ly6C^{+}CCR2^{+} inflammatory monocytes isolated from hind limb lymphatic-tissues or **D)** blood, derived from sham, *Bm*L3, *Bm*L3+αCCR2 or *Bm*L3+CL mice, 2dpi. Data in **D)** is reported as proportions of total white blood cells (WBC) (n=4 sham & *Bm*L3, n=3 *Bm*L3+αCCR2 & *Bm*L3+CL). **E)** Representative PDE images of sham, *Bm*L3, *Bm*L3+anti-CCR2 and *Bm*L3+CL mice, 6dpi. Yellow boxes highlight ICG retention **F)** aberrant lymphatics, **G)** hind-limb ICG retention and **H)** Evan's Blue dermal retention in sham, *Bm*L3 or *Bm*L3+αCCR2 / +CL treated mice, 6dpi (n=5 Sham & *Bm*L3, n=4 *Bm*L3+αCCR2 & *Bm*L3+CL). **I)** Representative epi-fluorescent images of lymphatic vessels and **J)** average lymphatic vessel aperture in sham, *Bm*L3, *Bm*L3+anti-CCR2 and *Bm*L3+CL mice, 6dpi (n=5 Sham & *Bm*L3, n=4 *Bm*L3+αCCR2 & *Bm*L3+CL). Scale bar 200μm. Data is from a single experiment. Histograms are mean ±SEM. Significance is indicated as *=P<0.05, **=P<0.01, ***=P<0.001, derived from a one-way ANOVA with Tukey's multiple comparisons post-hoc test.

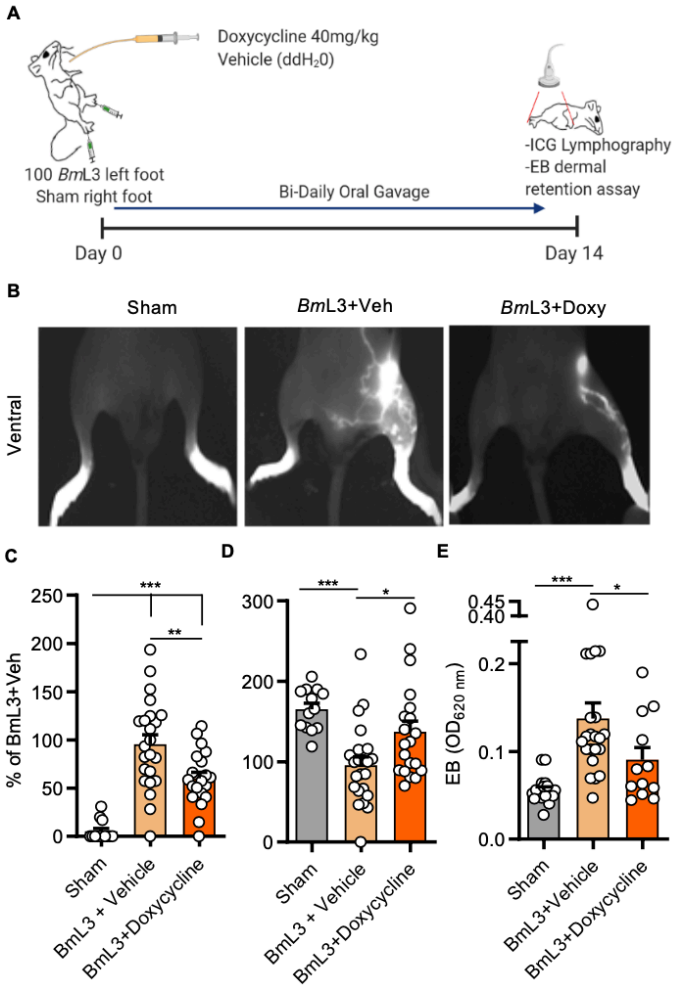
A
Doxycycline 40mg/kg
Vehicle (ddH2O)
100 BmL3 left foot
Sham right foot
Bi-Daily Oral Gavage
-ICG Lymphography
-EB dermal
retention assay
Day 0
Day 14
B
Sham
BmL3+Veh
BmL3+Doxy
Ventral
C
% of BmL3+Veh
Sham
BmL3 + Vehicle
BmL3+Doxycycline
D
Sham
BmL3 + Vehicle
BmL3+Doxycycline
E
EB (OD620 nm)
Sham
BmL3+Vehicle
BmL3+Doxycycline

939

Figure 8 *Doxycycline administration significantly ameliorates filarial lymphatic pathology.* **A)** Schematic of doxycycline intervention in *Bm*L3-infected C57BL/6J mice. **B)** Representative images, **C)** aberrant lymphatics, **D)** hind-limb ICG dye retention in sham, *Bm*L3+vehicle or *Bm*L3+Doxycycline treated mice, 14dpi (n=13 Sham; n=23 *Bm*L3+Vehicle, n=20 *Bm*L3+Doxycycline). Data plotted is % change normalised to mean values of the *Bm*L3+vehicle control group in order to compare data pooled from independent experiments. **E)** Evan's Blue dermal retention from left hind-limb skin (n=18 Sham; n=21 *Bm*L3+Vehicle; n=11 *Bm*L3+Doxycycline). Data is pooled from 3 individual experiments. Histograms are mean ±SEM. Significance is indicated as *=P<0.05, **=P<0.01, ***=P<0.001, ns = not significant derived from a one-way ANOVA with Tukey's multiple comparisons post-hoc test.

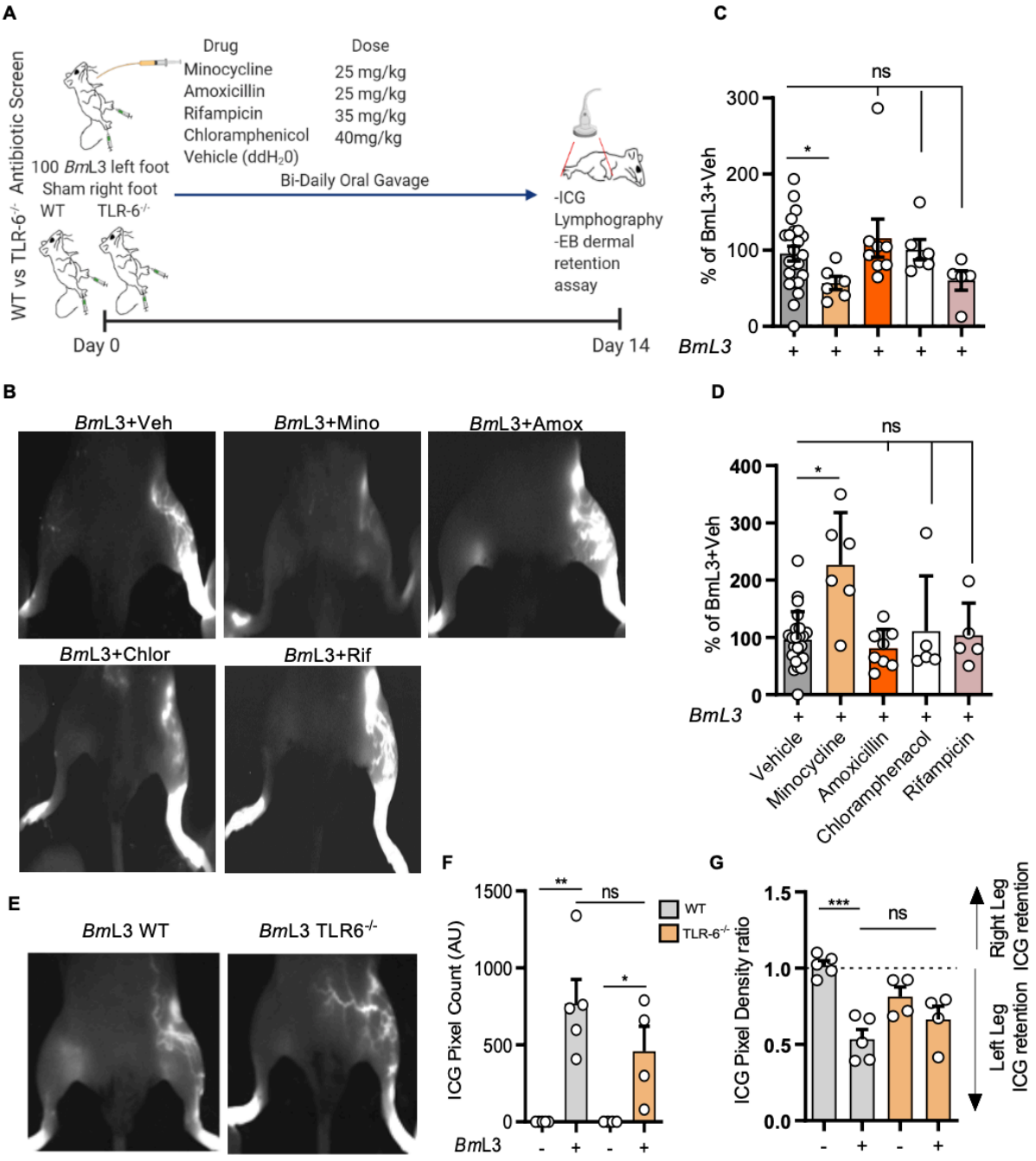
A
Antibiotic Screen
WT vs TLR-6-/-
Drug
Dose
Minocycline
25 mg/kg
Amoxicillin
25 mg/kg
Rifampicin
35 mg/kg
Chloramphenicol
40mg/kg
Vehicle (ddH20)
100 BmL3 left foot
Sham right foot
WT
TLR-6-/-
Bi-Daily Oral Gavage
-ICG Lymphography
-EB dermal retention assay
Day 0
Day 14
B
BmL3+Veh
BmL3+Mino
BmL3+Amox
BmL3+Chlor
BmL3+Rif
C
ns
*
% of BmL3+Veh
BmL3
D
ns
*
% of BmL3+Veh
BmL3
Vehicle
Minocycline
Amoxicillin
Chloramphenacol
Rifampicin
E
BmL3 WT
BmL3 TLR6-/-
F
**
ns
*
WT
TLR-6-/-
ICG Pixel Count (AU)
BmL3
G
***
ns
ICG Pixel Density ratio
Right Leg ICG retention
Left Leg ICG retention

Figure 9 *Doxycycline-mediated amelioration of filarial lymphatic pathology is independent of general antibiotic or anti-Wolbachia activity.*

A) Schematic for antibiotic screen and Toll-like receptor-6 knockout (TLR-$6^{-/-}$) experiments in *Bm*L3-infected C57BL/6J mice. **B)** Representative examples of PDE intravital imaging, **C)** aberrant lymphatics and **D)** ICG hind-limb retention in *Bm*L3-infected mice treated bi-daily with vehicle (*Bm*L3+Veh), minocycline (*Bm*L3+Mino), amoxicillin (*Bm*L3+Amox) chloramphenicol (*Bm*L3+Chlor) or rifampicin (*Bm*L3+Rif), 14dpi (n=23 *Bm*L3+Veh; n=6 *Bm*L3+Mino; n=8 *Bm*L3+Amox; n=6 *Bm*L3+Chlor; n=5 *Bm*L3+Rif). Data is % change normalised to mean of *Bm*L3+Veh mice in order to compare data pooled from independent experiments **E)** Representative examples of PDE intravital imaging, **F**) aberrant lymphatics and **G**) ICG hind-limb retention in WT or TLR-$6^{-/-}$ *Bm*L3-infected mice or corresponding sham-infection controls,14dpi (n=5 WT & TLR-$6^{-/-}$ sham; n=4 WT+*Bm*L3; n=6 TLR-$6^{-/-}$ +*Bm*L3). Data is pooled from 2 individual experiments (*Bm*L3+Amox in **C-D)** or a single experiment (*Bm*L3+Mino, *Bm*L3+Chlor, *Bm*L3+Rif groups in **C-D** and **F-G**) Histograms are mean±SEM. Significance is indicated as *=P<0.05, **=P<0.01, ns= not significant derived from a one-way ANOVA with Tukey's multiple comparisons post-hoc test.

970

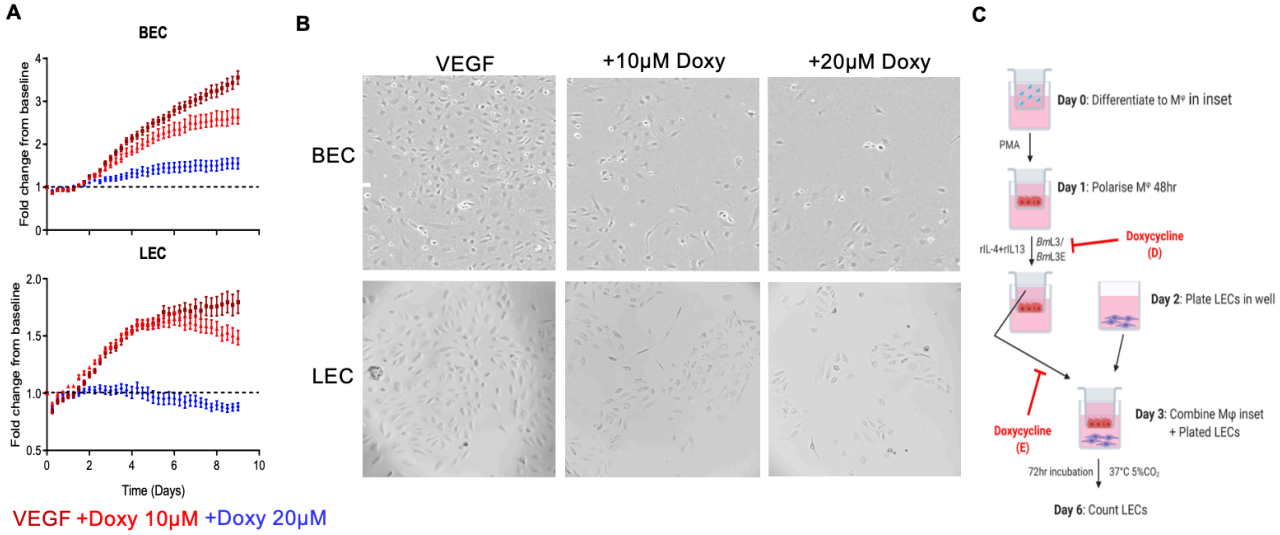
A
BEC
Fold change from baseline
LEC
Fold change from baseline
Time (Days)
VEGF +Doxy 10μM +Doxy 20μM
B
VEGF
+10μM Doxy
+20μM Doxy
BEC
LEC
C
Day 0: Differentiate to Mφ in inset
PMA
Day 1: Polarise Mφ 48hr
rIL-4+rIL13
BmL3/ BmL3E
Doxycycline (D)
Day 2: Plate LECs in well
Doxycycline (E)
Day 3: Combine Mφ inset + Plated LECs
72hr incubation
37°C 5%CO2
Day 6: Count LECs

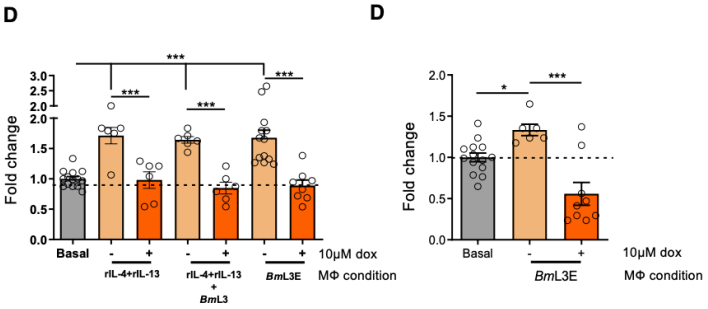
D
Fold change
Basal
rIL-4+rIL-13
rIL-4+rIL-13 + BmL3
BmL3E
10μM dox
MΦ condition

D
Fold change
Basal
BmL3E
10μM dox
MΦ condition

971

Figure 10 *Doxycycline inhibits LEC proliferation directly and via impairment of type-2 or filarial conditioned pro-lymphangiogenic Mϕ*

A) Blood Endothelial Cells (BEC) and LEC 9-day proliferation tracking following stimulation with 2ng/ml VEGF, with or without 10-20μM doxycycline. Data is fold-changes from initial BEC/LEC confluency. **B)** Representative images of BEC and LEC confluence at endpoint, scale bar=500μm. **C)** Schematic of Mϕ-LEC co-culture indicating where doxycycline was added. **D)** LEC enumeration following co-culture with MΦ pre-conditioned with: rIL-4+rIL-13, rIL-4+rIL-13+*Bm*L3 or *Bm*L3 extract (*Bm*L3E) with or without 10μM Doxycycline. **E)** LEC enumeration following co-culture with MΦ pre-conditioned with *Bm*L3E with/without 10μM Doxycycline. Histograms are mean ±SEM. Data is pooled from 2 individual experiments (**D,E**) or derived from a single experiment (**A**). Significance is indicated as *=P<0.05, ***=P<0.001, derived from a one-way ANOVA with Tukey's multiple comparisons post-hoc test.

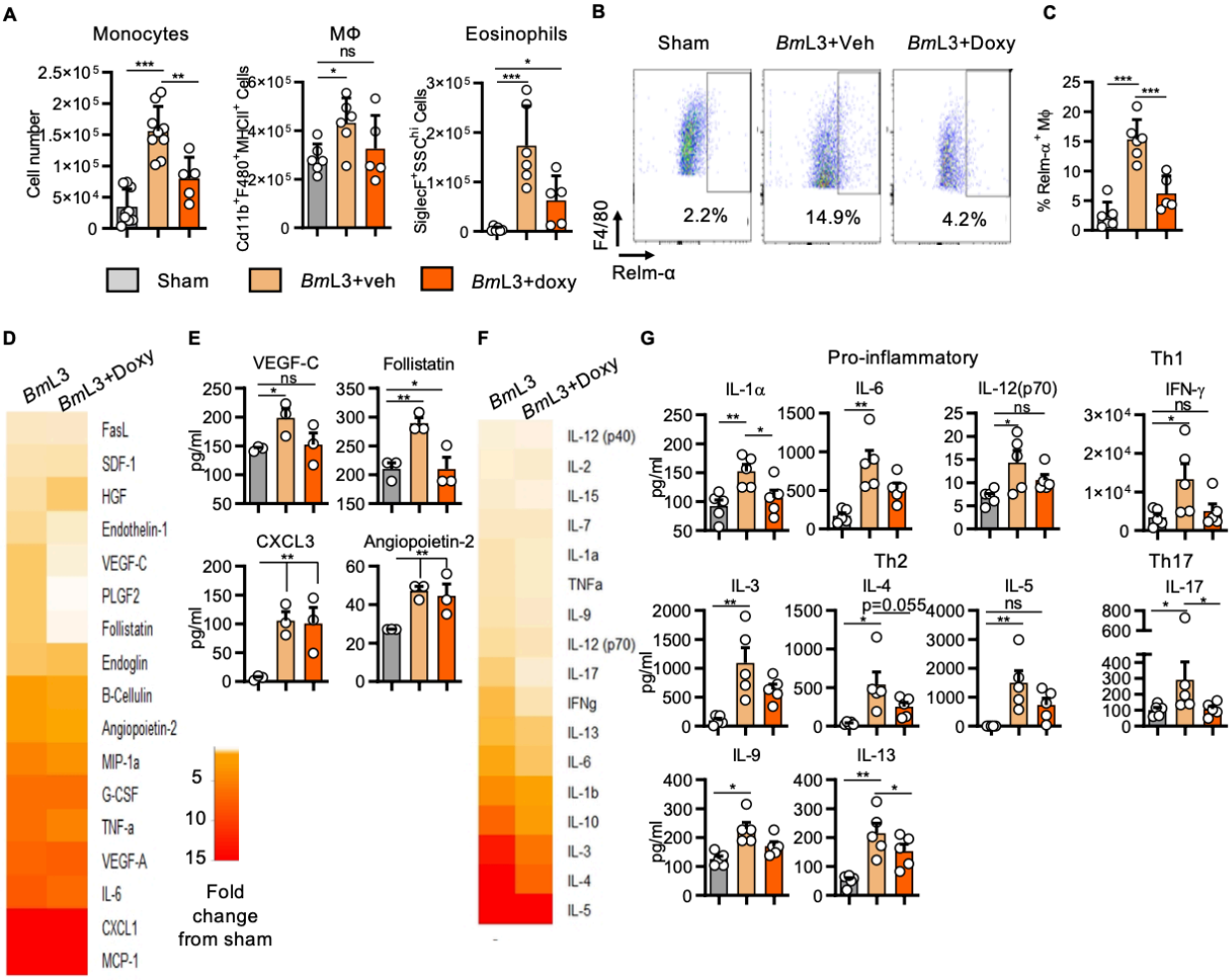
A
Monocytes
MΦ
Eosinophils
Cell number
Cd11b+F480+MHCII+ Cells
SiglecF+SSChi Cells
Sham
BmL3+veh
BmL3+doxy
B
Sham
BmL3+Veh
BmL3+Doxy
2.2%
14.9%
4.2%
F4/80
Relm-α
C
% Relm-α+ Mφ
D
BmL3
BmL3+Doxy
FasL
SDF-1
HGF
Endothelin-1
VEGF-C
PLGF2
Follistatin
Endoglin
B-Cellulin
Angiopoietin-2
MIP-1a
G-CSF
TNF-a
VEGF-A
IL-6
CXCL1
MCP-1
Fold change from sham
E
VEGF-C
Follistatin
CXCL3
Angiopoietin-2
pg/ml
F
BmL3
BmL3+Doxy
IL-12 (p40)
IL-2
IL-15
IL-7
IL-1a
TNFa
IL-9
IL-12 (p70)
IL-17
IFNg
IL-13
IL-6
IL-1b
IL-10
IL-3
IL-4
IL-5
G
Pro-inflammatory
Th1
Th2
Th17
IL-1α
IL-6
IL-12(p70)
IFN-γ
IL-3
IL-4
p=0.055
IL-5
IL-17
IL-9
IL-13
pg/ml

985

Figure 11 *Doxycycline ameliorates filarial lymphatic pathology by modulation of IL-4R-dependent inflammatory lymphangiogenesis*

A) immune cell populations from sdLN and surrounding lymphatics from C57BL/6J sham- or *Bm*L3-infected mice treated with vehicle or 40mg/kg doxycycline bi-daily, 14dpi. **B)** Representative flow cytometry plots and **C)** MΦ expression of Relm-α (n=6 Sham & BmL3+Veh; n=5 BmL3+Doxycycline). Cells were gated on live $CD11b^{+}MHCII^{+}F480^{+}$ cells. Data is Relm-α^{+} Mϕ as a proportion of total MΦ. **D)** Proteomic array of lymphangiogenic molecules in 72h cell cultures derived from sdLN and lymphatic tissues, 14dpi. Heatmap orange and red depict increasing fold-change compared with mean sham-infected mice **E)** lymphangiogenic molecules attaining statistical significance, data plotted per individual mouse (n=3 Sham, *Bm*L3 & *Bm*L3+Doxycycline) **F)**. Proteomic array of cytokine levels in splenocyte cultures 72h post-polyclonal re-stimulation with αCD3/CD28. Heatmap orange and red depict increasing fold-change compared with mean sham-infected measurement. **G)** Cytokine concentrations attaining statistical significance, grouped under type of adaptive immune response, data plotted per individual mouse (n=5 Sham, *Bm*L3 & *Bm*L3+Doxycycline). Histograms are mean ±SEM. Data is pooled 2 individual experiments (**A,C**) or derived from a single experiment (**E,G**). Significance is indicated as *=P<0.05, **=P<0.01, ***=P<0.001, ns=not significant derived from a one-way ANOVA with Tukey's multiple comparisons post-hoc test.